Battery and Flywheel hybridization of a reversible Pumped-Storage Hydro Power Plant for wear and tear reduction

Stefano Casarin[a,*], Giovanna Cavazzini[a], Juan Ignacio Pérez-Díaz[b]

[a] *Dept. of Industrial Engineering, University of Padova, via Venezia 1, 35131, Padova, Italy*
[b] *Dept. of Hydraulic and Energy Engineering, Escuela de Ingenieros de Caminos, Canales y Puertos, Technical University of Madrid (UPM), c/Profesor Aranguren s/n, 28040, Madrid, Spain*

Abstract

Energy security and environmental challenges are some of the drivers for increasing the electricity generation from non-programmable Renewable Energy Sources (RES), adding pressure to the grid, especially if located in weakly connected (or isolated) islands, like Sardinia. Variable-speed Pumped Storage Hydro Power (PSHP) can offer a high degree of flexibility in providing ancillary services (namely primary and secondary regulations), but due to the hydro-mechanical nature of the equipment, sudden variations in the power output cause wear and tear. Other energy storage devices cannot compete with PSHP in terms of energy and power availability. The aim of this research is to assess the benefits derived from the hybridization of a PSHP with Battery Energy Storage System (BESS) and Flywheel Energy Storage System (FESS), to be installed in the Sardinia island (Italy). A dynamic model of the hybrid plant was made in MATLAB–Simulink® environment. A detailed model of the variable-speed pump-turbine was obtained from experimental data, and a simplified model of a fixed-speed turbine was produced. A detailed FESS model was provided by CIEMAT (Madrid, Spain) and a simplified BESS model was included. A dedicated control strategy to manage the power flows and accounting for State Of Charge (SOC) control, was implemented. A total of 100 combinations of BESS and FESS powers were taken into account, and the control strategy was calibrated for each one of them. The plant was simulated open-loop over a 3600 s time period, feeding historical frequency and Automatic Generation Control (AGC) data. The simulations covered three PSHP operation modes: variable/fixed-speed turbine and variable-speed pump, and with/without hybridization. The performances of the hybridization were evaluated with wear and tear indicators for the PSHP (distance travelled by and number of movements of the wicket gate for turbine, fluctuations of the shaft torque for the pump) and capacity loss (life consumption) for the BESS. The results show that all the combinations of BESS and FESS powers result in the reduction of both the travelled distance and number of movements of the guide vanes. The best hybrid combination for the PSHP does not affect the BESS life consumption, which still is always in an acceptable range. A comparison between the non-hybrid variable-speed turbine and the hybrid fixed-speed counterpart shows that the electric powers do not differ substantially, but the hybridization smooths the movement of the guide vanes. The pump torque fluctuations sharply decrease with the hybridization, but more research is needed to validate that the change in the fluctuation index corresponds to a physical phenomenon. Overall, the hybridization improves the plant performances in terms of wear and tear reduction, and the presence of an additional FESS benefits both the BESS and the PSHP. The results also highlight the necessity for more research in variable-speed pumps providing ancillary services, and their impact.

Keywords: frequency regulation, hybrid energy storage, pumped storage hydropower, lithium-ion batteries, flywheel energy storage system

Manuscript accepted – 11 June 2023 https://doi.org/10.1016/j.est.2023.108059

1. Introduction

In the last decades, emerging environmental concerns have resulted in an increase of electricity generation from Renewable Energy Sources (RES), which have arisen to the 13.6 % of the world primary energy production [1]. New RES installations for electricity generation (wind, photovoltaic (PV) power plants) are mostly non-dispatchable, leading to higher needs for frequency regulation services to maintain the stability of the grid [2]. In this context, Pumped Storage Hydro Power (PSHP) is the mature technology with the lowest ratio between cost and energy storage capacity [3, 4]. The recent breakthroughs in power electronics, leading to the possibility to operate conventional pump-storage units at variable speed, have extended the flexibility of PSHP, resulting in: i) a wider operational range, ii) higher hydraulic efficiencies compared to the fixed-speed counterparts, and iii) a faster transition to a new operating point, making them more capable to follow the rapid fluctuations of the system frequency [5–8]. In having the runner (and the electric machine rotor) decoupled from the grid frequency, the rotating masses cannot contribute to the grid inertia. This limitation can be overcome with proper tuning and programming of the induction machine controller, in order to provide synthetic inertia [9, 10].

Nevertheless, in either binary or ternary configurations, pumped-storage units need tens of seconds for switching from standstill to turbine or pump mode, and from one operating mode to another, a time span several orders of magnitude longer than that of the frequency fluctuations and often incompatible with the Transmission System Operator (TSO) guidelines [11, 12].

Besides its limitations (e.g. high capital investment, scarcity of suitable sites for new installations), PSHP is the leading energy storage technology in terms of installed power and capacity [13], but other energy storage technologies have and are rapidly spreading, with interesting features for the provision of ancillary services. Two notable examples are Battery Energy Storage Systems (BESSs) and Flywheel Energy Storage Systems (FESSs).

BESSs have already been studied for their abilities to provide frequency regulation services [3, 14–25]. Several technologies exist (lead acid, flow, lithium-ion, just to name a few), that differ for the employed materials, energy density, resistance to ageing, etc. Lithium-ion batteries enjoy high energy density, low self-discharge rates (less than 5 % on a monthly basis) and more than 1500 cycles of useful life [26, 27]. Extensive research has been performed on BESS in the last decades, leading to a sharp reduction in capital investment, improvements in energy density and useful life [28, 29].

FESS convert electrical energy into mechanical energy by setting in motion a rotor placed in a vacuum chamber and equipped with superconducting or magnetic bearings, in order to reduce the friction losses [30]. Contrary to BESSs, FESSs have a very low energy density and higher self-discharge losses, but enjoys a very high power density and can sustain a very high number of charge and discharge cycles [4, 26, 31–35]. Little information is available regarding modern FESS, which may exhibit lower self-discharge rates with due research and improvement of the bearings [36].

Clearly, there is not an energy storage technology that has every feature required to guarantee the stability of the grid frequency and to provide every ancillary service needed. The lack of a unique technology capable to solve every grid stability issue have led to the idea to hybridize not only storage and generation systems, but also different storage systems in order to exploit the advantages of each technology while compensating the respective disadvantages.

Moghaddam and Chowdhuryhave proposed a method to find the optimal size (for mitigating wind power fluctuations) of a PSHP-BESS plant according to the discrete Fourier transformation of the historical data of the power imbalance caused by Wind Turbine Generators (WTGs): the PSHP is sized according to the low frequency components, whereas the BESS according to the higher [37]. Guezgouz et al. developed an efficient energy management strategy and an algorithm to determine the optimal size of an hybrid battery-PSHP storage system situated in a remote location with only wind and solar power generation [38]. Anindito

*Corresponding author

Email addresses: stefano.casarin.3@phd.unipd.it (Stefano Casarin), giovanna.cavazzini@unipd.it (Giovanna Cavazzini), ji.perez@upm.es (Juan Ignacio Pérez-Díaz)

et al. have assessed the economical benefits of including BESS into a PSHP under different scenarios of RES penetration and ecological constraints [39]. More recently Makinen et al. modelled a combined BESS-hydropower plant participating in the Frequency Containment Reserve (FCR) balancing reserve market in the Nordic Power System to assess the plant ability to fulfill its requirements [18]. Finally, Valentín et al. studied the benefits of the hybridization of a 35 MW run-of-river Kaplan unit with a small size (650 kW) BESS providing FCR in Germany. The presence of the BESS reduced both the runner and the blades servomotors mileage, which is found to be proportional to the wear and fatigue damage, respectively [40].

Besides BESS, some works have focussed on hydro-FESS integration: Makarov et al. modelled and simulated a hydro plant hybridized with FESS. The hybrid configuration proved to be feasible and to provide a robust and accurate frequency regulation services, with the FESS taking the most of the regulation task in terms of variability, thus reducing hydro wearing and tearing problem. Later on, Lu et al. have validated the aforementioned findings via experimental tests [41, 42]. A frequency control strategy was developed for an isolated insular power system with 100 % RES generation. The hybrid controller (hydro and flywheels) aims at maintaining stable the grid frequency and reduce the hydros and FESS wear, while tracking the variable-speed wind turbines rotational speed deviations and the FESS State Of Charge (SOC) [43].

Flywheels, co-operating with BESS, contribute to smooth the power generated by the RESs, help to stabilize microgrids in islanded mode, and lead to an extension of BESS life [44–51].

Akin to FESSs, supercapacitors (SCs) have also been studied in hybrid configurations, either with hydropower plants [52, 53] or with BESSs, smoothing the RESs power output [54–56] or provide frequency regulation services [25, 57–64]. This technology was not included in the present study, in favour of FESS, due to their current higher capacity costs [35, 65], even though these are expected to fall in the future, making it more competitive [4].

Regardless of the employed technology, the hybridization of energy storage devices implies the coupling of a "slow" unit with a "fast" unit. A key element of such an hybrid configuration is the control strategy, that manages the power flows and the SOC of each unit.

Jin et al. have developed an optimized algorithm to coordinate a "slow" and a "fast" unit, whose purpose is to efficiently distribute in real time the load between the two; another strategy, among the control variables, which considers the SOC of the storage devices has been proposed [66, 67]. Laban has modeled a hydropower plant coupled with a BESS for the provision of primary frequency control in the Nordic Power System, proposing two different control strategies and comparing them on the basis of the hydro wear and tear and the BESS life consumption due to cycling [68]. Other works have presented different control strategies for either frequency regulation services and RES power smoothing [41, 43, 49, 63, 69–71].

A common trait of the aforementioned works is that the Hybrid Energy Storage Systems (HESSs) are made of two technologies. Kheawcum and Sangwongwanich have proposed a storage system made of three devices – hydro, BESS, and FESS – for providing primary frequency control to the electric grid of a small island with high PV penetration, operating in islanded mode [72]. Low-pass filters with different time constants split the regulation effort between the PSHP (the slowest), the BESS, and the FESS (the fastest), though the control strategy does not take the SOC into account. Moreover, the study does not include an analysis on the wear and tear induced by the regulation effort and its possible mitigation due to the hybridization.

The idea to hybridize a PSHP with more than one energy storage device is interesting as the few hybrid power plants with hydro generation and energy storage are equipped with BESS. BESSs have been integrated in a few existing hydro plants so as to improve the plant's performance in the frequency control ancillary services while reducing the wear and tear of the turbine's wicket gates. However, it is acknowledged in the literature that cycle ageing is more severe for battery cells than for other storage technologies such as flywheels and SCs. Actually, hybrid battery-SC energy storage systems have been proposed in quite a few papers as an effective solution to smooth wind and solar PV power variations. The control strategy proposed (or assumed) in such papers consists basically in splitting the input signal of the energy management system (renewable power) into a low- and high-frequency components which are then used as input signals to the BESS and supercapacitor storage control, respectively. The control strategy used in the few existing hybrid hydro-battery projects is analogous: the system's frequency signal is split into low- and high-frequency components which are then used as input signals of the hydro and BESS control, respectively. Batteries are

better suited than a hydro unit to track the high-frequency component of the system's frequency signal, but worse than flywheels or SCs. However, the energy storage capacity of a FESS is usually rather lower than that of BESS. Hydro units are slower than both BESS and FESS but can help keep the BESS and FESS' SOC under control.

Moreover, new and emerging regulation services are being studied and implemented. In recent years, the Italian TSO TERNA introduced the "Pilot Project Ultra-rapid frequency regulation service" [73]. The participation in this service (and the access to the respective revenue stream) is subordinated to the commitment of 5 MW to 25 MW and their availability for 1000 h per year. In "Fast Reserve" operation, the unit must automatically deliver the committed power for the primary regulation within 1 s from the beginning of the event (activation within 300 ms), maintain the power input/output for 30 s, and then de-ramp. Hybridizing a "slow" unit (PSHP) with "fast" (BESS) and "very fast" (FESS) units would allow for the participation in such services. Moreover, new regulations may arise in the future, requiring stricter obligations in the provision of ancillary services. Finally, during the regular plant operation, the FESS and BESS together can relieve the burden of fast and frequent power adjustments from the PSHP, both improving the stability of the grid and the equipment lifetime.

The aim of this study is to evaluate a HESS abilities to provide a wide range of regulation services, and assess the benefits (if any) derived by the hybridization of a PSHP with BESS and FESS.

The case-study, as well as the design data of the hydro power plant, were taken from the feasibility studies of a yet-to-be realized seawater pumped storage hydro plant (sPSHP), to be installed in Foxi Murdegu, on the eastern coast of the Sardinia island [74–76]. A sPSHP employs an artificial upper reservoir located on a cliff, and the sea as lower reservoir. Such a plant takes advantage of the infinite water availability of the sea and the reduced investment costs deriving from realizing only one artificial reservoir. This solution has first been tested with success in Japan, and it was proved that its main drawbacks can be tackled with the existing technology [77, 78]. The corrosion due to the usage of seawater, and the relative issues have been neglected in this study, as out of the scope of the analysis. The plant is expected to participate in primary, secondary, and tertiary regulation services, as well as providing fast services that are not codified yet. So far the analysis has been limited to primary and secondary regulation services, leaving the study of the other services for future works. The results can be extended to regular PSHPs.

The variable speed technology grants a high degree of flexibility compared to the fixed speed pump-turbines counterparts. Given the large capital investments for such a project, a practical approach would be to either realize a HESS with a fixed-speed PSHP, or a non-hybridized variable-speed PSHP. The analysis performed in this study proposes a comparison between the four possible configurations: fixed/variable-speed PSHP with/without hybridization.

The most relevant original aspects of this work are hereby enumerated:

- the hybrid topology considered in the paper includes three energy storage devices: PSHP, BESS, and FESS. Many works focus on the hybridization of a hydropower plant with BESS (Refs. [18, 37–40]), few address the hydro-FESS hybridization (Refs. [41, 42]) or the hydro-SC hybridization (Refs. [52, 53]). Other works study the integration of BESS with FESS (Refs. [44, 46–51]), BESS with SC (Refs. [25, 57–64]). Only Ref. [72] addressed the hybridization of a hydropower plant with BESS and FESS, but the authors do not consider the impact of the proposed hybridization on the equipment (namely the wear and tear and the BESS degradation due to cycling) and the SOC of the BESS and FESS. The hydropower plant considered in [72] is a mini hydropower pl

- This study employs a detailed model of the reversible pump-turbine hydraulic machine, whose characteristic curves have been reconstructed from experimental data sampled from a real machine. In most papers in the literature, generic equations are used to represent the hydraulic behaviour of a turbine [79], and these equations do not consider the limits in the operating range due to unstable behaviour and cavitation. The authors of Ref. [72] do not provide details about the model they use to reproduce the performance of the considered small hydropower plant. From the information provided in their paper, one can assume that they used PowerFactory library models.

- The control strategy to allocate the power flows between each component of the hybrid plant (PSHP,

BESS, FESS) takes into account the frequency components of the frequency regulation signal, and the SOC levels of the BESS and FESS. Ref. [72] does not consider the contribution of the hydropower plant to control the SOC level of the BESS and FESS.

- In the paper we consider the provision of primary and secondary frequency regulation by a variable-speed pump-turbine operating in pump mode. The papers cited in the literature which have studied the hybridization of a PSHP with another energy storage device [37–39, 71] consider only the operation of the PSHP in turbine mode.
- The analysis in this paper adopts the plant owner's point of view, assessing the impact of the hybridization in the reduction of the wear and tear indicators, one of the most relevant issues for the operation of PSHP in providing frequency regulation services. Moreover, while there is a consensus that the equipment degradation indicators for a turbine or a pump-turbine operating in pump mode are the movements of the wicket gate blades, no established methodologies are present in the literature to evaluate the wear and tear of variable-speed pumps or pump-turbines operating in pump mode. This work proposes an indicator to estimate the wear and tear of the variable-speed pump-turbine when it operates in pump mode.

The following sections are structured as follows: Section 2 outlines the case study upon which this analysis has been performed; Section 3 gives a description of the dynamic model of each component, as well as the control strategy of each energy storage device in the HESS and the procedures adopted for the wear and tear estimation; Section 4 describes the simulations that were performed and the calibration process; eventually, in Section 5 the results are presented and commented.

2. Case study

The Sardinia island is electrically connected to the mainland via two HVDC submarine cables: the SAPEI (500 kV, 1000 MW), and the SACOI (200 kV, 300 MW). As of 2019, the gross electrical energy generation comes from thermo-electric power plants (2386.1 MW_e), hydro (466.4 MW_e), wind turbines generators (1054.9 MW_e), and PV generators (872.6 MW_e) [80].

The HESS under study would help stabilize the local grid by participating in the primary and secondary regulation. The tertiary regulation is not part of this work.

2.1. Regulatory framework

The Italian grid code (*Codice di Rete*, [81]) mandates that every generating unit (*unità di produzione*, UP) whose "efficient power" (*potenza efficiente*) is greater than 10 MW_e must provide primary regulation – FCR. The term "efficient power" is defined as "the maximum active power that the UP can generate in continuity, for thermoelectric power plants, or for a certain amount of hours for hydropower plants". In this sense, *efficient power* can be interpreted as "rated power". For consistency with the local regulations, the term "efficient power" is going to be used for the rest of this work. The efficient power is among the technical specifications that the plant owner must declare during the (mandatory) registration process in the Generating Units Registry (RUP), and is used to quantify both the FCR and Frequency Restoration Reserve (FRR). The provision of secondary regulation – FRR – is not mandatory and, contrary to the primary, is remunerated, given that the UP fulfills the requirements. The Foxi Murdegu HESS will participate in both FCR and FRR, and therefore must: a) have a permanent droop set to 0.04; b) commit a minimum FCR of 10 % of the efficient power (upwards and downwards); c) deliver at least 50 % of the FCR (with the maximum possible gradient) within 15 s from the beginning of the frequency perturbation (when the frequency deviation exceeds the deadband boundaries), 100 % within 30 s; d) not limit its response unless due to hydraulic conditions, energy availability, and regulation devices' intrinsic properties e) commit a minimum FRR of 15 % of the efficient power (if participating in the service).

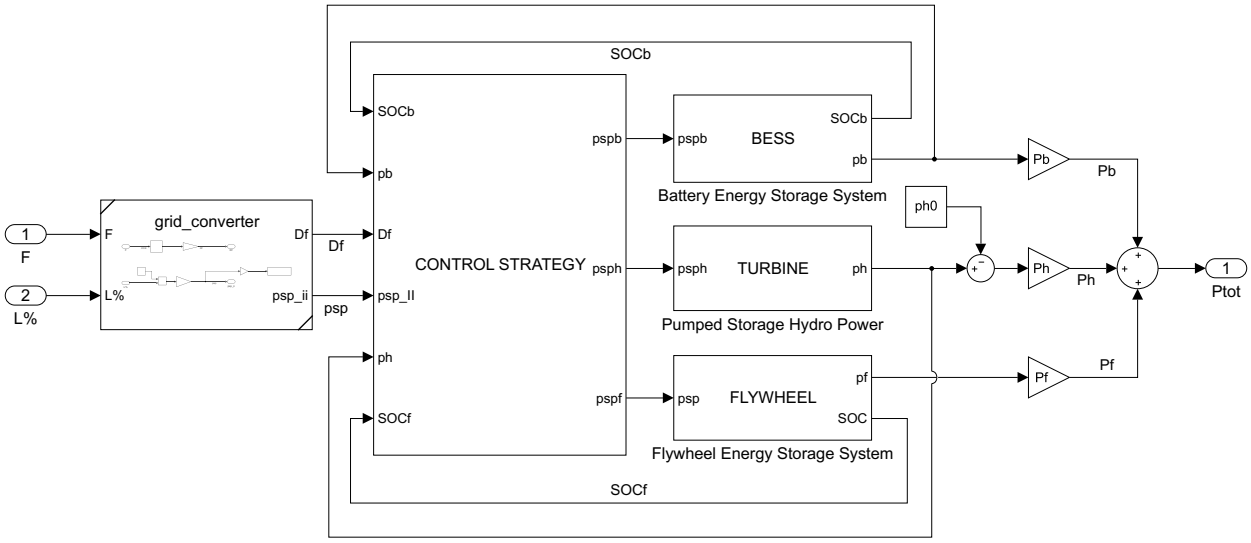

Figure 1: Block diagram of the HESS (variable-speed turbine). Conceptually, the pump and fixed-speed turbine do not entail any meaningful difference.

3. Dynamic model

Foxi Murdegu PSHP main design features have been obtained from preliminary pre-feasibility and feasibility studies [74, 75]. According to these, the plant shall be equipped with a variable speed reversible pump-turbine, coupled with a Doubly Fed Induction Generator (DFIG). In the fixed speed operation cases considered in the paper, the same hydraulic machine is assumed to be coupled with a synchronous electrical motor/generator.

Together with the hydro, the hybrid plant model includes a BESS and a FESS bank, each equipped with its own power converter.

The model has been developed in the MATLAB – Simulink® environment [82]. Figure 1 shows a high-level block diagram that helps to understand the inputs and outputs of the control strategy we propose to determine the active power set-point (psp) of the three elements in the studied hybrid power plant: pumped-storage unit, BESS and FESS.

When the PSHP is hybridized, the BESS and FESS can be considered as *section* of the power plant, similarly to the vapour circuit of a combined-cycle power plant. This does not violate the grid code regulations. The hybrid power plant is considered as a hydro power plant whose *efficient power* is defined as the sum of the rated powers of the equipment:

$$\hat{P}_{eff} = \hat{P}_h^b + \hat{P}_b^b + \hat{P}_f^b. \tag{1}$$

The subscripts (h,b,f) stand for *hydro*, *battery*, and *flywheel*, respectively, the superscript (^{b}) indicates the quantity expressed is a base for the per-unit notation, the hat accent ($\hat{}$) indicates that the quantity expressed is in absolute value.

Both the FCR and FRR imply a change in output/input power, which is controlled by a psp. In particular, each regulation psp can be calculated as:

$$\overline{psp}_I = -\frac{\Delta f}{\sigma}, \tag{2}$$

$$\overline{psp}_{II} = 2 \cdot \overline{SB} \cdot \frac{L_{\%} - 50}{100}, \quad L_{\%} \in [0, 100]\,, \tag{3}$$

where Δf is the frequency error (p.u.), σ the permanent droop, $\overline{SB}$ the power reserve for the secondary regulation (p.u.), and $L_{\%}$ the signal sent by the AGC and received by the plant participating in the service.

The subscripts (I, II) refer to the primary and secondary regulations, respectively, the bar accent ($\bar{}$) indicates that the quantity is expressed in p.u., system-base (s.b.), whereas its absence implies that the same quantity is in p.u., machine-base (m.b.).

The following paragraphs present the model equations of each element of the system under investigation.

3.1. Pumped-storage hydropower plant

The PSHP model is made of a total of 5 elements: i) upper and lower reservoirs, ii) penstock, iii) one variable-speed pump-turbine equipped with a iv) speed governor, coupled with v) one DFIG/synchronous machine.

3.1.1. Reservoirs and penstock

The lower reservoir is the sea, its water capacity is infinite and it is assumed that the water level is constant over time. The upper reservoir, according to the pre-feasibility studies, has a capacity of $1.016 \times 10^6\,\mathrm{m}^3$.

Mass and momentum conservation laws fully describe the transient flow in the conduit [83]. An elastic water column model was employed, and a lumped parameters approach was used to transform the aforementioned conservation laws into ordinary differential equations [71, 84, 85]. The approach consists in splitting the conduit into consecutive segments and distribute its properties evenly across the segments. After a preliminary sensitivity analysis, $n_{ge} = 3$ segments have been chosen. The flowrate q_i as well as the head h_i at the end of the i-th segment are calculated with:

$$\frac{dq_i}{dt} = \frac{n_{ge}}{T_w}\left(h_{i-1} - h_i - \frac{f_p}{n_{ge}}\left|q_i\right| q_i\right), \quad T_w = \frac{L}{gA}\frac{\hat{Q}^b}{\hat{H}^b} \tag{4}$$

$$\frac{dh_i}{dt} = \frac{T_w n_{ge}}{\left(L/a_p\right)^2}(q_i - q_{i+1}), \tag{5}$$

where T_w (s) is the water starting time, $\hat{Q}^b$ (m^3/s) and $\hat{H}^b$ (m) are respectively the base flowrate and head, f_p (p.u.) is the friction coefficient, L (m) the penstock length and a_p (m/s) the penstock wave speed.

The friction coefficient for hydraulic losses f_p was obtained by calculating the Darcy friction factor for fully developed turbulent flow and assumed constant, with a roughness coefficient ϵ equal to 0.3 mm (tar-coated steel pipes, new) [86].

3.1.2. Variable speed pump-turbine

The analytical representation of a turbine is often done with generic equations [87–89].

In one of the pre-feasibility studies, the pump-turbine performances were deducted from the characterization of a variable-speed pump-turbine machine made by the University of Padova [75]. In this analysis it was assumed that, according to the similitude theory, the characteristic curves of the machine can describe Foxi Murdegu pump-turbine operation.

The experimental points were provided in the non-dimensional coordinate system $(\hat{\psi}, \hat{\phi}, \hat{\eta})$, pressure number, flow number, and efficiency, respectively. For turbine mode, the position of the wicket gate blades $\hat{\alpha}$ (deg) was also provided for each sampled point. Every coordinate is transposed in per-unit notation (with the respective bases $\hat{\alpha}^b, \hat{\psi}^b, \hat{\phi}^b, \hat{\eta}^b$). In most of the literature, hydraulic machines' characteristic curves are expressed in the (n_{11}, q_{11}) coordinate system, whereas in this work, as well as in fluid mechanics, the notation (ψ, ϕ) is adopted. Thanks to the per-unit notation, the change of reference system is straightforward, as shown in (8) and (9).

$$\psi = \frac{h}{n_h^2}, \tag{6}$$

$$\phi = \frac{q}{n_h}, \tag{7}$$

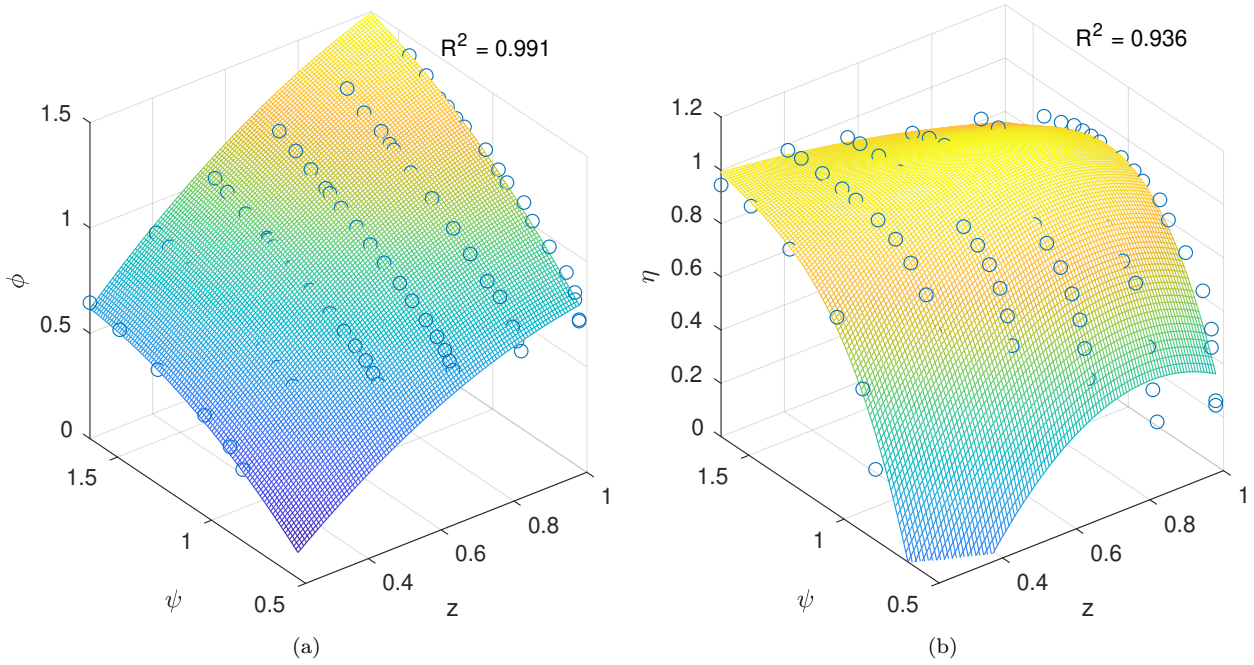

Figure 2: Turbine mode: flow number (a) and efficiency (b) characteristic curves. The experimental points are marked with circles. All quantities are in per unit.

$$q_{11} = \frac{q}{\sqrt{h}} = \frac{\cancel{n_h}\phi}{\cancel{n_h}\sqrt{\psi}} = \frac{\phi}{\sqrt{\psi}}, \tag{8}$$

$$n_{11} = \frac{n_h}{\sqrt{h}} = \frac{\cancel{n_h}}{\cancel{n_h}\sqrt{\psi}} = \frac{1}{\sqrt{\psi}}. \tag{9}$$

It is worth to point out that the formal definition of the pressure and flow numbers include physical (such as g) and geometrical (e.g. the machine outer diameter) constants that are elided with the per-unit notation. In either mode the characteristic curves were obtained by polynomial interpolation of the experimental points. In turbine mode the fitting coefficients are the result of a constrained linear optimization problem. The objective function – to minimize – is the sum of squared errors. The variables to be optimized are the polynomials' coefficients (c_{ij}, d_{ij}), subject to a concavity constraint in the dominion: as the real operation of a turbine is a concave phenomenon, such has to be the polynomial representing it. The concavity constraint was not necessary for pump mode. The graphic representation of the characteristic curves for turbine and pump mode, along with the experimental points, are presented in Figures 2, 3, and as equations (10) and (11), being η_t and η_p (p.u.) the hydraulic efficiency respectively in turbine and pump mode, (e_i, f_i) the polynomial coefficients for the characteristic curves in pump mode, and z (p.u.) the wicket gate position.

$$\phi_t = \sum_{i=0}^{2}\sum_{j=0}^{2} c_{ij} \cdot z^i \cdot \psi^j, \qquad \eta_t = \sum_{i=0}^{2}\sum_{j=0}^{3} d_{ij} \cdot z^i \cdot \psi^j, \tag{10}$$

$$\psi_p = \sum_{i=0}^{3} e_i \cdot \phi^{3-i}, \qquad \eta_p = \sum_{i=0}^{6} f_i \cdot \phi^{6-i}. \tag{11}$$

Thanks to the per-unit notation, both head and flowrate can be easily converted into pressure and flow

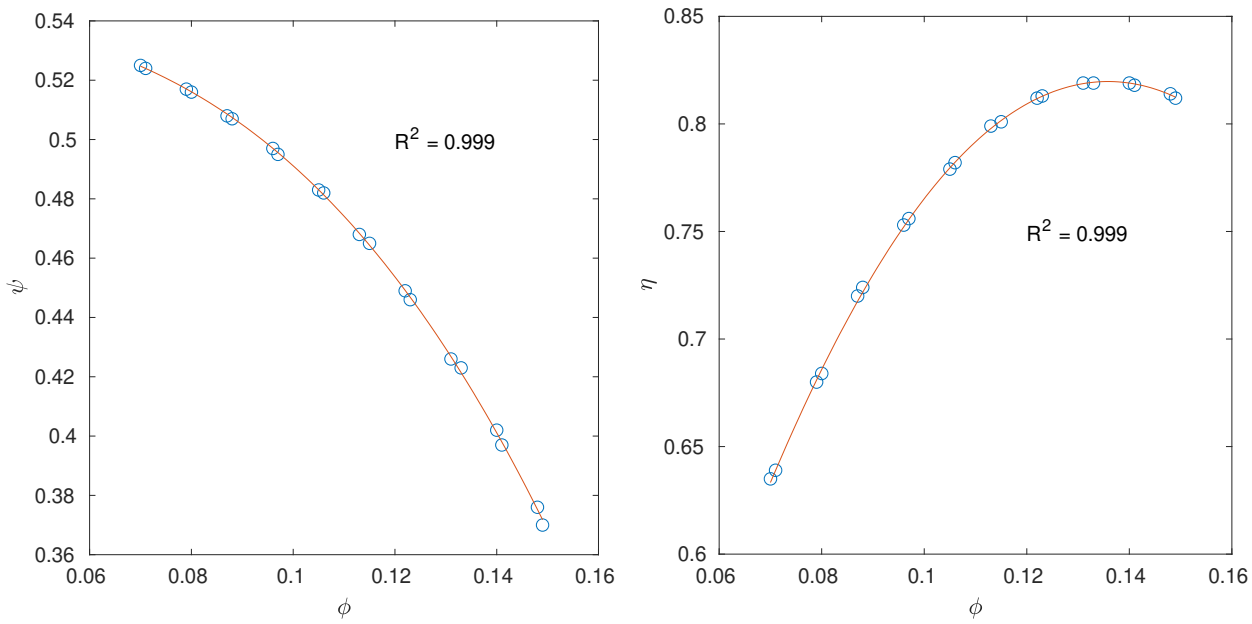

(a) (b)

Figure 3: Pump mode: pressure number (a) and efficiency (b) characteristic curves. The experimental points are marked with circles. All quantities are in per unit.

numbers and vice/versa, via the runner rotational speed n_h (p.u.):

$$h = \psi_k \cdot (n_h)^2 \qquad q = \phi_k \cdot n_h, \qquad k \in \{t, p\}. \tag{12}$$

The mechanical power at the shaft, in turbine and pump modes, is calculated as:

$$p_{mech.} = \begin{cases} \eta_t hq, & q > 0 \\ \frac{1}{\eta_p} hq, & q < 0 \end{cases} . \tag{13}$$

According to the manufacturer's data sheet, the variable speed pump-turbine has an operating range of 472 rpm to 577 rpm, with rated speed set at 525 rpm.

3.1.3. Synchronous generator

In the European market, the closest synchronous machine rated speed in that range is 500 rpm. In this work, the same hydraulic machine is assumed to be installed in either the fixed and variable-speed operation.

In fixed-speed operation, a simplified model of the generator was employed, as the goal of this study is to assess the plant ability to deliver active power [90].

The synchronous generator model is based on the assumption that the mechanical power (p_{mech}) is equal to the electrical power (p_h) (14), and that the rotor speed is exactly synchronized to the grid frequency (15).

$$p_h = p_{mech}, \tag{14}$$

$$\Delta n_h = \Delta f. \tag{15}$$

3.1.4. Doubly Fed Induction Generator

The DFIG interacts mechanically with the pump-turbine and electrically with the grid. These two phenomena are modelled separately. The mechanical interaction between the DFIG and the pump-turbine

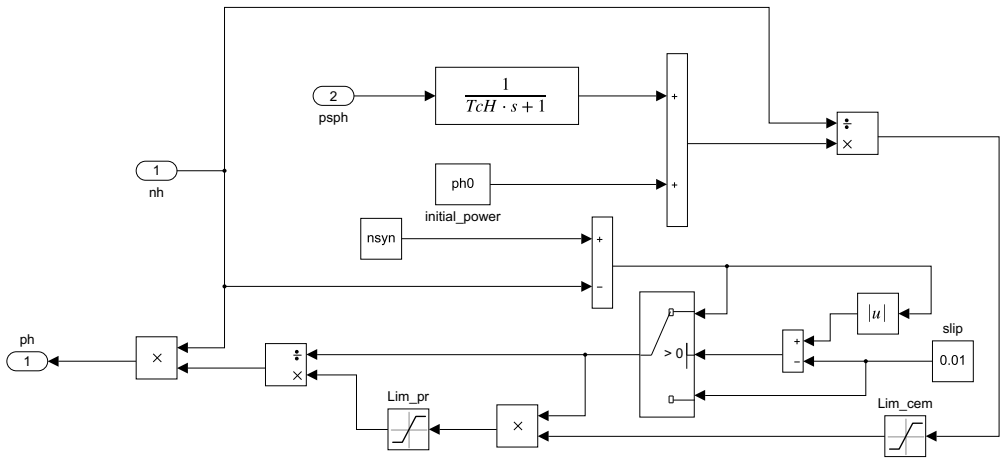

Figure 4: DFIG block diagram.

shaft is represented with equation (16).

$$T_m \frac{dn_h}{dt} = (p_{mech} - p_h) \frac{1}{n_h}, \tag{16}$$

T_m (s) being the generator mechanical starting time (s) and p_h (p.u.) the electrical power sent to the grid. With regards to the electrical interaction (Figure 4), the DFIG absorbs/releases power in accordance to the control signal psp_h received by the Grid Side Converter (GSC), which is assumed to behave as a first order transfer function with time constant T_{cH} (s) [91]. The Rotor Side Converter (RSC) governs the electromagnetic torque c_{em} [92], which is calculated from the input variables (n_h and the psp_h) neglecting the generator losses. The speed deviation from the synchronous speed ($n_{syn} = \pm 1$ p.u.), minus the generator slip, is used to calculate the active power at the rotor, p_r, from which the active power p_h is obtained. Both the electromagnetic torque and the power at the rotor are limited by two saturator blocks.

3.1.5. Speed governor

The difference between the conventional fixed and variable-speed pump-turbine also reflects on the modelling of the speed governor, whose task is to adapt the wicket gate position to correct a speed error (variable speed) or a power-frequency error (fixed speed).

In pump mode, the wicket gate plays no role in the operation, and it is assumed that it has no influence on the hydraulic efficiency. For this reason, the speed governor is modelled only for the turbine.

A control signal (CS) is generated by a Proportional Integral (PI) controller and fed to a servomotor, which responds with a first-order lag with a T_s (s) time constant (17). The guide vane servo is assumed to operate a regulating ring, and a backlash proposed by Saarinen et al. is applied [93].

The next two paragraphs illustrate how the control signal is calculated in variable and fixed speed operation, respectively.

Variable speed. The control strategy for the turbine power output was taken from [94], having the rotational speed as control variable. A controller with proportional and integral gains, respectively $k_{p,var}$ and $k_{i,var}$, elaborates the speed error Δn_h and produces a control signal (18).

The reference rotational speed can be chosen following different criteria. Being the focus of this study a comparison between different kinds of hybridization of fixed and variable-speed PSHP, this value was set to be the runner rated speed and kept constant throughout the simulation.

Fixed speed. In fixed-speed operation, the PI controller receives as input a power-frequency error signal, Eq. (19), made of the runner speed deviation Δn_h and the power error. A deadband of 10 mHz (0.0002 p.u.)

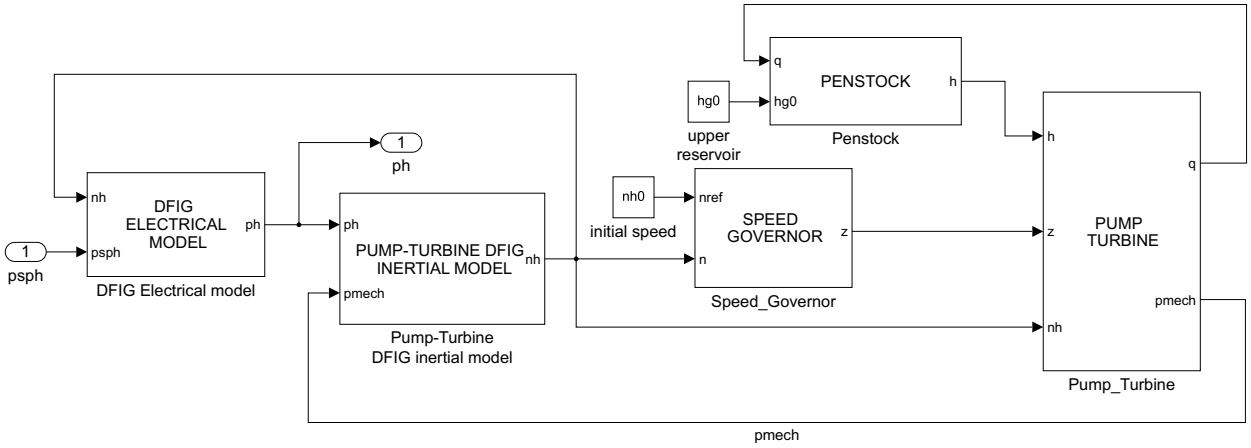

Figure 5: Block diagram of the PSHP modules and their connections.

is applied to the speed error signal, according to [81, 95]. The power error is the sum of the scheduled generated power, p_h^0, the control signal for power generation, p_h^*, and the electrical power currently being generated p_h with negative sign (all quantities in p.u.). p_h^* is obtained by the control strategy, as seen in Section 3.4.2, whereas in the non-hybridized case it corresponds to the secondary regulation psp signal, psp_{II}.

$$\Delta z = \frac{1}{T_s \cdot s + 1} CS_{var/fix}, \tag{17}$$

$$CS_{var} = \left(k_{p,var} + \frac{k_{i,var}}{s} \right) \Delta n_h, \tag{18}$$

$$CS_{fix} = \left(k_{p,fix} + \frac{k_{i,fix}}{s} \right) \left[\Delta n_h - \sigma_h \left(p_h^0 + p_h^* - p_h \right) \right]. \tag{19}$$

The complete block diagram of the PSHP model and its component is presented in Fig. 5.

3.1.6. Pump-turbine wear estimation

As stated in Section 1, the aim of this work is to assess the advantages derived from the hybridization of the PSHP with BESS and FESS in providing ancillary services. One of the advantages can be the hydraulic machine reduced wear and tear.

While the FESS wear and tear has been for now neglected, two algorithms to estimate the ageing process respectively of PSHP and BESS (presented in Section 3.2.1) have been implemented.

When studying the hybridization of a PSHP with a "fast" unit, the adopted perspective is often performance-oriented, meaning that the objective is to reduce power imbalances/increase the accuracy of the regulation services [18, 37, 52, 66] or the plant profitability [38, 39, 42]. Similarly, the adoption of variable-speed pump-turbines is assessed in terms of their ability to provide ancillary services [96–98], or in the improved performances with respect to their fixed-speed counterparts [7, 99].

In a Francis pump-turbine, the wear and tear can be measured or analyzed in various components, from different variables, and can be consequence of distinct operation maneuvers or events. A full characterization of the fatigue of a pump-turbine unit would require, in our opinion, a careful experimental work and the use of several sensors such as accelerometers, displacement transducers, strain gauges, force transducers, etc. On the other hand, the numerical characterization of the fatigue of a pump-turbine unit is limited per se: in order to quantify the pressure pulsations appearing in the pump-turbine runner a Computational Fluid Dynamics (CFD) model should be used, which is out of the scope of this research. Coupling a 3D model of the pump-turbine with a 1D model of the plant's conduits is not an easy task. The 3D model can be replaced

with a reduced order model (1D) properly calibrated from the former, or from experimental measurements. We think this is out of the scope of the study as well.

We chose to use a 1D model in the paper and adopt the approach suggested in [100]. This approach evaluates in a qualitative manner the wear and tear of a Francis turbine using the total distance (defined as the sum of the displacements) travelled by the guide vanes and their number of movements (defined as the instant in which the blades stop either because they have reached the target position or because their movement is inverted). The authors state that the approach is based in turn on previous researches by other authors working in the field of tribology. Since the publication of [100], some other authors have used the mentioned approach for the same purpose [40, 68, 101, 102].

A variable-speed pump can provide ancillary services (contrary to the fixed-speed counterpart), but to the authors' knowledge there are no established methodologies to assess the impacts of the provision of such services. Studies on variable-speed hydraulic machines' wear and tear tend to focus on the turbine mode [103, 104]; if not, they employ CFD or finite elements method, looking at the "microscopic" phenomena occurring in the machine [105–107]. The number of movements of the guide vanes and their travelled distance are not valid indicators to evaluate the wear and tear of the variable-speed pump-turbine operating in pump mode, since their position is assumed to be invariable during the provision of primary and secondary regulation. All this considered, we propose a new method to assess the quality of the operation of the variable-speed pump in providing ancillary services: by considering the torque at the shaft (this quantity has been used in the literature for analogous purposes [108, 109]), we assume that its fluctuations are directly related to the wear and tear of the equipment, by computing the Mei-Wang Fluctuation Index (MWFI) [110] of the respective signal: $\hat{T}_{mech} = \hat{P}_{mech}/\hat{N}_h$.

This fluctuation index combines the standard deviation with the rotation angle θ of a signal here defined as a collection of N data points of the type (x, y), x being the time instant and y the recorded value (the mechanical torque in this case):

$$
\begin{aligned}
\text{MWFI} &= \sqrt{\frac{1}{N}\sum_{i=1}^{N}(y(i)-\bar{y})^2} \times \sum_{i=1}^{N}\theta_i \\
\theta_i &= \begin{cases} \arctan|k_i| & i = 1 \text{ or } N \\ |\arctan k_i - \arctan k_{i-1}| & 2 \le i \le N-1, \text{ and } k_i \times k_{i-1} \ge 0 \\ \arctan|k_i| + \arctan|k_{i-1}| & 2 \le i \le N-1, \text{ and } k_i \times k_{i-1} < 0 \end{cases} \\
k_i &= \begin{cases} \frac{y(i+1)-y(i)}{x(i+1)-x(i)} & 1 \le i \le N-1 \\ \frac{y(N)-y(N-1)}{x(N)-x(N-1)} & i = N \end{cases},
\end{aligned}
\tag{20}
$$

Here, $\bar{y}$ refers to the mean value of the y series. The MWFI was preferred for its ability to detect fluctuations in processes where classical indices fail (zigzag, sine/cosine processes, with different numbers of repetitions) [110].

3.2. Batteries

The chemical phenomena are assumed to be at least one order of magnitude faster than the electrical ones [111]. For this reason, and given the time scale of the grid ancillary services considered in this paper, the chemical phenomena have been neglected. The electrical phenomena mainly correspond to the power converter and have therefore been modelled by eq. (21) [68], where $T_{del,b}$ represents the time delay of the measurement and control circuits and T_{cB} represents the time necessary for the converter to deliver the active power p_b from the psp signal psp_b.

$$
p_b = \frac{1}{T_{cB} \cdot s + 1} e^{-sT_{del,b}} psp_b. \tag{21}
$$

During its operation the BESS SOC varies according to the energy stored/released and is calculated by taking into account the round-trip efficiency η_{rt} (assumed constant) of the charge/discharge processes and

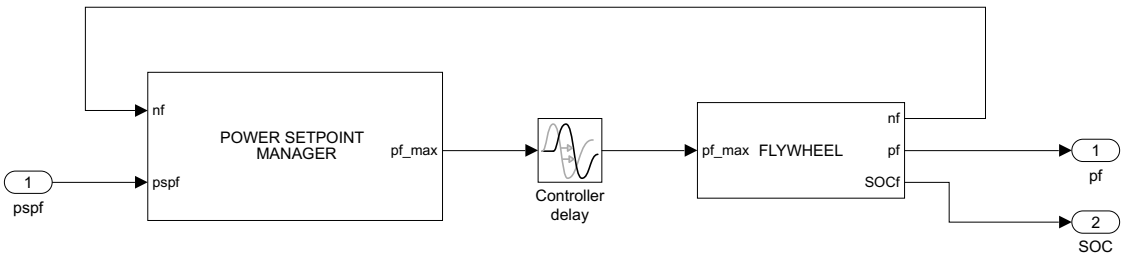

Figure 6: Block diagram of the FESS

the device capacity (defined by the energy-to-power ratio, EP_{ratio}):

$$SOC_b = -\frac{1}{EP_{ratio}} \cdot \begin{cases} {\eta_b}^{0.5} \frac{1}{s} p_b, & p_b < 0 \\ {\eta_b}^{-0.5} \frac{1}{s} p_b, & p_b > 0 \end{cases} \quad ; \quad SOC_b \in [0, 1]. \tag{22}$$

The list of the BESS parameters, together with their values, is presented in Table 1.

3.2.1. BESS ageing estimation

Batteries' degradation by idling (calendar ageing) is neglected, taking only into account the life consumption due to cycling.

According to Stroe et al. [112], the BESS cycling degradation depends on the mean SOC value $SOC_{b,avg}$, the number of the charge/discharge cycles nc, and their depth cd. For a Li-ion battery bank operating at 25 °C:

$$C_{loss} = 0.021 e^{-0.01943 SOC_{b,avg}} \cdot cd^{0.7612} \cdot nc^{0.5}. \tag{23}$$

The SOC signal outputted from the simulation is processed by the Rainflow algorithm that returns the number, depth, and average SOC of the equivalent cycles [113]. Miner rule for mechanical fatigue [114] is used for estimating the combined capacity loss for each equivalent cycle the BESS has gone through:

$$LC_b = \sum_j \frac{nc_j}{nf_j}, \tag{24}$$

$$nf_j = \left[\frac{0.2}{0.021 e^{-0.01943 SOC^b_{avg,j}} \cdot cd_j^{0.7612}.} \right]^2. \tag{25}$$

The number of j-th cycles that lead to the BESS end of life presented in (25) are calculated using (23) by setting the capacity loss equal to 20 %, the industry standard for BESS end of life. The result is the per-unit life consumption LC that the BESS bears during the simulated period. The base quantity for the BESS cells life has been chosen the number of hours in 10 years operation, 87.6×10^3 h.

3.3. Flywheel

The model for the FESS was adapted from the "ACEBO" model developed by CIEMAT (Madrid, Spain) [47, 115, 116]. This flywheel has metallic rotor (placed in a vacuum chamber) and is equipped with hybrid angular contact ball rotor bearings with an additional magnetic levitation system. The electrical machine is a 6/4 switched reluctance machine coupled with a three half-bridge IGBT converter. The device was designed to have a rated (maximum) power of 25 kW. The rotor speed range is 6000 rpm to 9000 rpm, guaranteeing that the FESS usable energy is 50 % of the total rotor energy, a common practice in the design of flywheels [47]. The energy capacity is 869.2 Wh, meaning that the design C_{rate} is 28.76 kW/kWh.

The block diagram is presented in Fig. 6.

The "Power Set-point Manager" calculates the maximum power the FESS can deliver $p_{f,max}$ according to the rotor rotational speed n_f via eq. (26). The power output p_f is equal to the power set-point $p_{psp,f}$, unless

	Parameter	Value	Unit
BESS	EP_{ratio}	1	kWh/kW
	$\hat{\eta}_{rt}$	0.9	(–)
	T_{cB}	0.3	s
	$T_{del,b}$	0.1	s
FESS	a_1	4.0824	p.u.
	a_2	−9.5191	p.u.
	a_3	8.5572	p.u.
	a_4	−2.0744	p.u.
	$\hat{\eta}_f$	0.82	(–)
	I	15.5	N m^2
	$\hat{N}_{max}$	9×10^3	rpm
	$\hat{N}_{min}$	6×10^3	rpm
	$\hat{P}^b_{1f}$	25	kW
	$T_{del,f}$	0.1	s
	$\hat{T}_{loss}$	0.07	N m

Table 1: BESS and FESS model parameters.

it exceeds the maximum power, in which case the power output is $p_f = p_{f,max}$.

$$p_{f,max} = \sum_{i=1}^{4} a_i \cdot n_f^{4-i}, \tag{26}$$

The power converter is modeled as a simple time delay (see "Power Converter" block in Fig. 6), i.e. the power converter follows the active power set-point calculated in the the "Power Set-point Manager" block with a time delay $T_{del,f}$. The "Flywheel" block calculates the flywheel rotational speed and SOC according to (27) and (28) respectively. Moreover it contains the logical apparatus that controls the power flows according to the SOC (e.g. if the SOC is 0 the power output can only be negative, meaning only the recharge is possible), and the FESS inertial model equation.

$$n_f = \frac{1}{s}\frac{\hat{T}^b}{I\hat{\omega}^b}\left(-\frac{p_f}{\hat{\eta}_f \cdot n_f} - \frac{\hat{T}_{loss}}{\hat{T}^b}\right), \tag{27}$$

$$SOC_f = \frac{n_f^2 - n_{min,f}^2}{n_{max,f}^2 - n_{min,f}^2}, \tag{28}$$

$$\hat{T}^b = \frac{\hat{P}^b_{1f}}{\hat{\omega}_b}; \quad \hat{\omega}_b = \frac{\pi \hat{N}_{f,max}}{30}.$$

$\hat{\omega}^b$ is the base angular velocity (rad/s), $\hat{P}^b_{1f}$ is the rated power of a single module (25 kW), $\hat{T}^b$ is the base torque (N m), I the moment of inertia (kg m^2), $\hat{\eta}_f$ is the round-trip efficiency (assumed constant), $\hat{T}_{loss}$ (N m) represents the self-discharge losses as a resistant torque, $n_{min,f}$ and $n_{max,f}$ (p.u.) are the rotational speed bounds. The list of the parameters, together with their values, is presented in Table 1.

A single FESS module rated power is 25 kW: it is common practice to install several modules so that their cumulative powers achieve the desired power capacity. Model-wise this would be the ideal approach: as seen in (26) the model is not completely linear. On the other hand, including hundreds of blocks like the one in Fig. 6 raises the computation times to unfeasible levels. For this reason, one scaled FESS model has been used.

3.4. Control strategy

The control strategy in a HESS determines how the regulation effort of the FCR and FRR is split among the PSHP, BESS, and FESS. The criterion is to have the fastest devices (FESS and BESS) to take care of the high frequency components while the PSHP deals with the low ones, a strategy called "Frequency Split" [68].

Moreover, given its power and energy availability, the PSHP should have the task to control both BESS and FESS SOC, by increasing or reducing its power output.

The control strategy therefore is made of two elements: the SOC control component, and the division of the regulation effort between the different technologies. While in variable-speed operation the PSHP active power generation can be controlled at will, the synchronous motor/generator is strictly coupled to the grid, and the active power control is performed at the speed governor level, by acting on the p_h^* term of Eq. (19).

The following paragraphs present the SOC control and regulation management implementations, respectively.

3.4.1. SOC control

It is important for the PSHP to control the SOC of both BESS and FESS in order to avoid either device to be fully charged (discharged), resulting in the unavailability to provide upwards (downwards) regulation services, and reduce the ageing of the BESS due to cycling.

The SOC control algorithm of either BESS and FESS is the same as in [66], with the difference that the inner bounds are defined as the outer plus/minus a fixed band, ΔSOC. The psp sent to control the PSHP for BESS/FESS SOC is null as long as the BESS/FESS SOC is inside the lower and upper bounds $SOC^L_{b/f}$ and $SOC^U_{b/f}$) respectively. As soon as $SOC \leq SOC^L_{b/f}$ ($SOC \geq SOC^U_{b/f}$), $psp^{SOC}_{b/f}$ assumes a positive (negative) constant value, until the SOC reaches the value of $SOC^L_{b/f} + \Delta SOC$ ($SOC^U_{b/f} - \Delta SOC$).

When SOC control is active, $psp^{SOC}_{b/f} = ci_{b/f}$, where ci is the "charge intensity" with which BESS and FESS are charged/discharged. This value is in per-unit with respect to the device rated power, and an appropriate base change is performed.

3.4.2. FCR and FRR management

Both the BESS and FESS are equipped with their own power converter, which controls the power output according to the psp that it is fed. In this configuration there are two low-pass filters, for the PSHP and BESS respectively.

$$\overline{psp}_f = (\overline{psp}_I + \overline{psp}_{II}) - (\overline{p}_h - \overline{p}_h^0) - \overline{p}_b, \tag{29}$$

$$\overline{psp}_b = \frac{1}{T_{lpf,b}s + 1}(\overline{psp}_I + \overline{psp}_{II}) - (\overline{p}_h - \overline{p}_h^0) + \frac{1}{T_{lpf,h}s + 1}\overline{psp}_f^{SOC}. \tag{30}$$

Eq. (29) is used to calculate the FESS psp, $\overline{psp}_f$, in system base, as the unfiltered (droop-based) primary and secondary psps, $\overline{psp}_I$ and $\overline{psp}_{II}$ respectively, minus the power that it is currently being delivered by the PSHP and BESS, respectively.

The BESS psp is generated according to eq. (30). The primary and secondary required powers are filtered with its low-pass filter with time constant $T_{lpf,b}$ (s), to which the PSHP active power variation is subtracted. The last term in the equation includes the PSHP SOC control psp for the FESS, filtered with the same time constant as the PSHP: $T_{lpf,h}$ (s). This is to make sure that the power meant to control FESS SOC is not absorbed by the BESS.

In variable-speed operation, the PSHP control signal is generated akin to the BESS and FESS, as it is elaborated by the GSC, whereas in fixed-speed operation the signal becomes part of the power-frequency error elaborated by the speed governor PI controller.

$$\overline{psp}_h = \frac{1}{T_{lpf,h}s + 1}\left(\overline{psp}_I + \overline{psp}_{II} + \overline{psp}_b^{SOC} + \overline{psp}_f^{SOC}\right) + \frac{T_d s}{T_{fnf}s + 1}\Delta f, \tag{31}$$

$$\overline{p}_h^* = \frac{1}{T_{lpf,h}s + 1}\left(-\overline{psp}_I T_{lpf,h}s + \overline{psp}_{II} + \overline{psp}_b^{SOC} + \overline{psp}_f^{SOC}\right). \tag{32}$$

As shown in (31), the sum of the primary, secondary, and SOC control psp are filtered out from their rapid components. The last term pertains to the synthetic inertia control action, with a T_d (s) derivative gain and T_{fnf} (s) time constant for the noise filter [9, 10].

In fixed-speed operation only the speed governor power-frequency error can be controlled. Instead of placing a low-pass filter, the fast components of the grid frequency (corresponding to the FCR psp) must be subtracted. This is easily seen in (32), as the first term in the brackets: the primary regulation psp filtered with a high-pass filter with the same time constant as the low-pass filter of the secondary and SOC control psps.

The appropriate base-changes are actuated to each psp, before it is fed to the corresponding energy storage device.

4. Simulations

The model presented in Section 3 is simulated open-loop, due to the lack of a detailed model of the Sardinian electric system and the power imbalance events that characterize it. Frequency and AGC input signals are fed as inputs, and the plant power input/output variation is collected.

The variable-speed PSHP is simulated in both turbine and pump mode, whereas the fixed-speed is simulated only in turbine mode, as the pump cannot provide FCR nor FRR in the first place, so it was not simulated.

In every simulation it is assumed that, at $t = 0$: i) the grid frequency is 50 Hz, the AGC control signal, $L_{\%}$, is 50 (no secondary regulation); ii) the PSHP is in steady state, and iii) is consuming/generating the power committed in the day-ahead market, while iv) the BESS and FESS have a null power input/output, and both of their SOC is 50 %. In turbine mode, since the model was developed to be applied even in different case studies, the runner initial and reference rotational speeds can be decided by the user, and in this work they are both set to their rated value (525 rpm in variable speed, and 500 rpm in fixed speed); in variable-speed pump operation the rotational speed depends on the defined power input and the water level at the upper reservoir: the initial power input is chosen so the resulting rotational speed is the rated value, whereas the water level is the same as in turbine mode. The initial quantities of the pump-turbine are presented in Table. 2. The adoption of numeric tolerances to calculate the initial quantities of the turbine operation lead to minimum discrepancies in the values of $\hat{H}_{g0}$.

Indeed, it has been verified that 3600 s of turbine operation at rated power would decrease the level to 1.0197 p.u.. Similarly, after one hour of operation in pump mode, the water level would increase to 1.0427 p.u.. This small change in the per-unit values of the geodetic water level justifies the choice to keep the value constant during the simulations.

Real historical data from the Sardinian electric grid was not available, therefore the frequency and AGC signal for continental Italy was used (Figure 7). It was chosen to simulate 1 h (3600 s) starting from 04:28:17 of January 21, 2020, the recorded hour containing the most intense frequency deviation (over 150 mHz), and beginning at the instant with no recorded frequency error.

The frequency sampling resolution is 20 ms, the AGC signal is 1 min, linearly interpolated to cover for the missing values.

The PSHP was simulated first without hybridization, and then considering that $\hat{P}_{b/f}$ could assume values in the range of 0.5 MW to 5 MW $\{0.5, 1, 1.5, \ldots, 5\}$ MW and testing all the 100 combinations. The search was limited to the power rating, excluding the energy capacity: the BESS power capacity was fixed as a parameter to 1 MWh/MW, whereas the FESS model used in this study had a fixed speed range (6000 rpm to 9000 rpm).

Obviously the hybrid plant control depends on the power ratings of both BESS and FESS, therefore the model control parameters had to be properly calibrated. The next section describes the model calibration process.

Table 2: Initial conditions of the PSHP, in both turbine (variable and fixed speed) and pump mode. $\hat{H}_{g0}$ and $\hat{H}_0$ are in (m), $\hat{Q}_0$ in (m^3/s), $\hat{N}_0$ in (rpm), $\hat{\alpha}_0$ in (°), $\hat{\eta}_0$ in %, and $\hat{P}_0$ in (MW). All the other quantities are in (p.u.)

	Turbine		Pump		Turbine		Pump
	Variable	Fixed	Variable		Variable	Fixed	Variable
$\hat{H}_{g0}$	366.98	366.97	367.00	h_{g0}	1.0322	1.0322	1.0322
$\hat{Q}_0$	27.58	26.86	−31.63	q_0	0.5628	0.5482	−0.6456
$\hat{H}_0$	363.34	363.52	371.78	h_0	1.0220	1.0225	1.0457
$\hat{N}_0$	525.00	500.00	−525.20	n_0	1.0000	0.9524	−1.0004
$\hat{\alpha}_0$	12.60	11.80	–	z_0	0.3738	0.3500	–
$\hat{\eta}_0$	79.42	81.50	79.54	η_0	0.9971	1.0232	0.9986
$\hat{P}_0$	80.00	80.00	−94.292	p_0	0.5736	0.5736	−0.6760

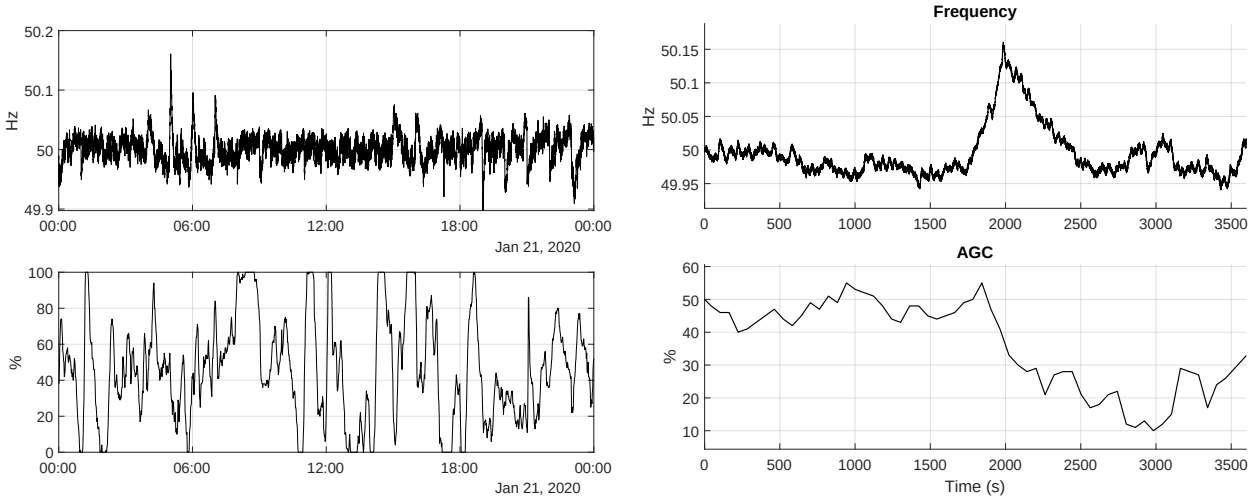

(a) (b)

Figure 7: Recorded frequency (top) and AGC signal (bottom) for January 21, 2020 (a), and detail of the simulated hour (b).

Table 3: Variable speed operation: values of $T_{lpf,h}$ (s) for each combination of hybridizing BESS and FESS powers (MW). These values are identical for either turbine or pump mode.

$\hat{P}_f \backslash \hat{P}_b$	0.5	1	1.5	2	2.5	3	3.5	4	4.5	5
0.5	11.19	13.52	15.71	17.95	20.28	22.71	25.33	28.18	31.28	34.75
1	12.95	15.19	17.38	19.66	22.09	24.61	27.42	30.47	33.80	37.56
1.5	14.62	16.81	19.09	21.42	23.95	26.66	29.66	32.90	36.56	40.66
2	16.28	18.52	20.85	23.33	25.95	28.85	32.04	35.56	39.56	44.04
2.5	17.95	20.23	22.66	25.28	28.09	31.18	34.61	38.47	42.80	47.80
3	19.62	22.04	24.57	27.33	30.37	33.71	37.42	41.61	46.42	51.94
3.5	21.42	23.90	26.61	29.57	32.80	36.42	40.47	45.09	50.42	56.61
4	23.28	25.90	28.80	31.95	35.47	39.37	43.85	48.94	54.89	61.84
4.5	25.23	28.04	31.09	34.52	38.33	42.61	47.56	53.23	59.89	67.84
5	27.28	30.28	33.61	37.28	41.47	46.18	51.66	58.03	65.60	74.74

Table 4: Variable speed operation: values of $T_{lpf,b}$ (s) for each combination of hybridizing BESS and FESS powers (MW). These values are identical for either turbine or pump mode.

$\hat{P}_f \backslash \hat{P}_b$	0.5	1	1.5	2	2.5	3	3.5	4	4.5	5
0.5	8.79	8.79	8.84	8.84	8.84	8.84	8.84	8.84	8.84	8.79
1	10.89	10.89	10.89	10.89	10.89	10.89	10.84	10.84	10.84	10.79
1.5	12.65	12.65	12.65	12.65	12.65	12.60	12.60	12.60	12.55	12.55
2	14.36	14.36	14.36	14.31	14.31	14.26	14.26	14.21	14.16	14.16
2.5	16.02	16.02	15.97	15.97	15.92	15.87	15.87	15.82	15.77	15.72
3	17.68	17.68	17.63	17.58	17.58	17.53	17.48	17.43	17.38	17.33
3.5	19.38	19.38	19.34	19.29	19.24	19.19	19.09	19.04	18.99	18.95
4	21.19	21.14	21.04	21.00	20.95	20.90	20.80	20.75	20.65	20.61
4.5	23.00	22.95	22.90	22.80	22.75	22.66	22.56	22.51	22.41	22.31
5	24.95	24.85	24.80	24.71	24.61	24.51	24.41	24.32	24.22	24.12

4.1. Model calibration

There are three sets of control parameters in the model: the gains of the turbine governor PI controller, ($k_{p,var/fix}k_{i,var/fix}$), the SOC control parameters, ($SOC^L_{b/f}, SOC^U_{b/f}, \Delta SOC_{b/f}, ci_{b/f}$), and the low-pas filters' time constants ($T_{lpf,h/b}$).

The first set of parameters is not related to the hybridization per-se, but rather to the operation of the PSHP: in both variable and fixed-speed operation the turbine governor gains were found iteratively and kept constant for the rest of the calibration process, as well as for each and every simulation (with and without hybridization).

The SOC control parameters do not influence the rapidity of the plant to deliver power. Their values are presented in Table 7 and are kept constant in each and every simulation.

The third and last set of control parameters, the low-pass filters' time constants, affect the plant ability to deliver the FCR in due time and their value is a compromise between the plant owner to slow down as much as possible the PSHP and BESS power ramps (to reduce respectively their wear and tear and life consumption), and the regulatory framework presented in Sec. 2.1.

Their calibration process was performed iteratively and separately for the PSHP and BESS. First, all the intentional delays were set to zero, SOC control was suppressed, and no FRR was used. A 200 mHz amplitude underfrequency step signal was fed to the system and SOC^0_f was set to 100 % (for the FESS to be able to deliver the maximum power). With this setup, the maximum allowable value of $T_{lpf,h}$ was found, which later was fixed as a parameter for the search of BESS maximum delay, $T_{lpf,b}$, and the results are presented in Tables 3, 4, 5, and 6, and their graphical representations are shown in Figure 8.

As expected, the higher BESS and FESS powers are, the slower both PSHP and BESS can be operated.

Table 5: Fixed speed operation: values of $T_{lpf,h}$ (s) for each combination of hybridizing BESS and FESS powers (MW).

$\hat{P}_f \backslash \hat{P}_b$	0.5	1	1.5	2	2.5	3	3.5	4	4.5	5
0.5	9.92	11.95	13.91	15.90	17.94	20.08	22.40	24.94	27.71	30.75
1	11.47	13.43	15.39	17.40	19.53	21.80	24.28	26.94	29.93	33.25
1.5	12.95	14.88	16.87	18.99	21.19	23.61	26.24	29.11	32.34	35.97
2	14.40	16.36	18.44	20.62	22.98	25.54	28.35	31.48	34.97	38.93
2.5	15.88	17.90	20.05	22.34	24.85	27.60	30.62	34.02	37.84	42.22
3	17.36	19.47	21.74	24.18	26.84	29.80	33.10	36.81	41.01	45.91
3.5	18.93	21.16	23.55	26.15	29.02	32.19	35.79	39.87	44.55	49.99
4	20.56	22.92	25.45	28.23	31.35	34.82	38.75	43.25	48.48	54.64
4.5	22.28	24.76	27.48	30.50	33.85	37.66	42.01	47.03	52.89	59.90
5	24.12	26.75	29.68	32.95	36.63	40.80	45.61	51.26	57.90	65.97

Table 6: Fixed speed operation: values of $T_{lpf,b}$ (s) for each combination of hybridizing BESS and FESS powers (MW).

$\hat{P}_f \backslash \hat{P}_b$	0.5	1	1.5	2	2.5	3	3.5	4	4.5	5
0.5	8.64	8.73	8.74	8.70	8.73	8.78	8.74	8.72	8.63	8.68
1	10.79	10.79	10.79	10.84	10.80	10.79	10.74	10.78	10.73	10.71
1.5	12.60	12.60	12.60	12.57	12.60	12.55	12.50	12.51	12.47	12.45
2	14.31	14.31	14.26	14.26	14.21	14.21	14.16	14.14	14.14	14.11
2.5	15.97	15.97	15.92	15.92	15.87	15.82	15.82	15.78	15.72	15.67
3	17.68	17.63	17.58	17.53	17.53	17.48	17.43	17.33	17.33	17.29
3.5	19.38	19.29	19.24	19.24	19.19	19.14	19.09	18.99	18.95	18.90
4	21.14	21.04	21.00	20.95	20.90	20.80	20.75	20.70	20.65	20.56
4.5	23.00	22.90	22.85	22.75	22.71	22.61	22.56	22.46	22.36	22.31
5	24.90	24.80	24.76	24.66	24.56	24.46	24.41	24.27	24.22	24.07

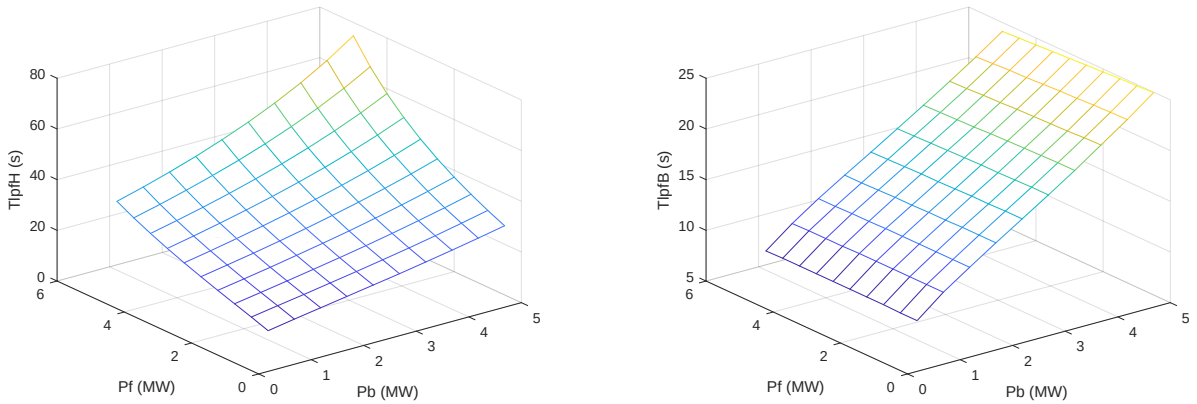

(a)

(b)

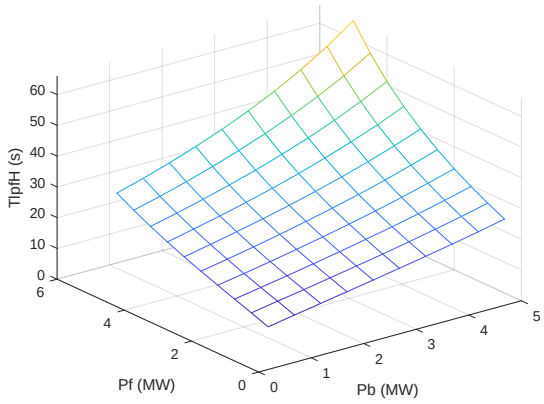

(c)

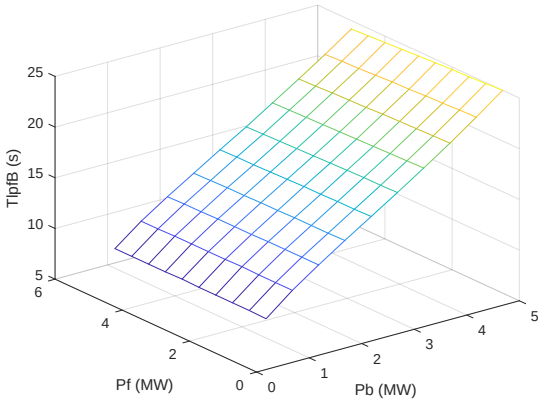

(d)

Figure 8: Low-pass filters' time constants for the variable-speed (top) and fixed-speed (bottom) plant. On the left-hand side: values of $T_{lpf,h}$; on the right-hand side: $T_{lpf,b}$

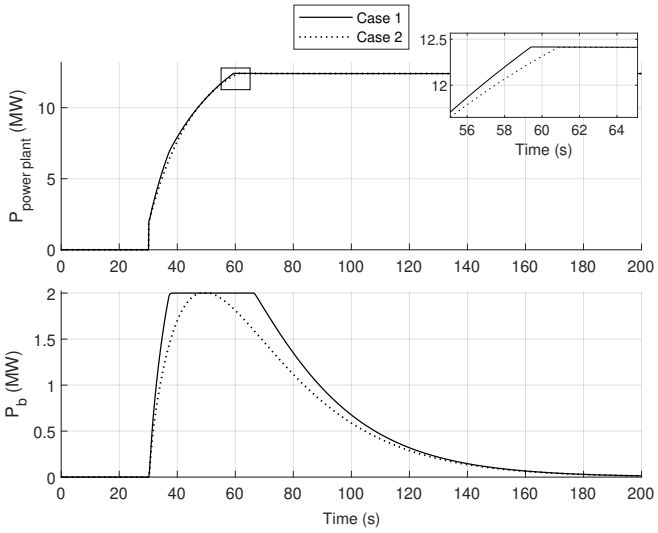

Figure 9: Active power comparison between two simulations: calibrated and incremented $T_{lpf,b}$ (Case 1 and 2 respectively).

Table 7: SOC control parameters.

	SOC^L (%)	SOC^U (%)	ΔSOC (%)	ci (p.u.)
BESS	40	60	10	0.8
FESS	20	80	10	0.8

At the same time, $T_{lpf,b}$ shows a slight dependency to the FESS power rating rather than its own. This is due to the architecture of the control strategy. Figure 9 shows the power plant, PSHP, BESS, and FESS powers after a step frequency deviation. The two simulated cases differ only for $T_{lpf,b}$, whose value in Case 2 is higher than in Case 1. It can be seen that, if $T_{lpf,b}$ is too high, the BESS will reduce its power before the plant output value has reached the correct value. The FESS in this case can't supply the additional power as its maximum power depends on its SOC.

5. Results

The results of the simulations for each configuration – variable-speed turbine, fixed-speed turbine, and variable-speed pump – are summarized in Figures 10, 11, 12, and 13 respectively. A red circle indicates the global minimum. Hereafter a "configuration" is a combination of installed BESS and FESS powers, and is indicated as $(\hat{P}_b, \hat{P}_f)$ MW.

In the variable-speed case, the reference case (non hybrid) for the turbine returns a distance travelled by the wicket gate blades, Lwg, equal to 0.7564 p.u., and a total of 137 movements (Nwg). The configuration (0.5, 0.5) MW is enough to reduce Lwg to 65.86 % (0.4984 p.u.) w.r.t the reference case and Nwg to 45.99 % (63).

While the maximum hybridizing power corresponds to the minimum Lwg (0.3202 p.u., 42.33 %, Figure 10a), there are 5 configurations that minimize Nwg, reducing it to 14.60 % (20) of the reference value. The most attractive among these, from the plant owner's point of view, would be the one with the minimal installed power (= minimal capital investment), corresponding to the configuration (4.5, 4) MW, with associated

Lwg of 43.34 % (0.3278 p.u.); the other configuration, (5, 3.5) MW, has a slightly superior Lwg: 44.55 % (0.3370 p.u.).

It is worth noting that the BESS and FESS installed powers impact the PSHP performance differently: configuration (5, 0.5) MW is associated with $Lwg = 0.3682$ p.u. and $Nwg = 24$, while configuration (0.5, 5) MW presents $Lwg = 0.4021$ p.u. and $Nwg = 29$. This difference is due to the FESS SOC control process. When the FESS rated power is 0.5 MW, the SOC control routine is triggered several times during one hour of operation (Figure 11a), where the PSHP adjusts its power output by 80 % of the FESS rated power: 0.4 MW. When the FESS rated power is maximum (5 MW), only one SOC control event occurs, but this entails a power adjustment by the PSHP of 4 MW (again 80 % of the FESS rated power), resulting in wider movements of the guide vanes.

The BESS life consumption LC_b, does not appear to be correlated with the low-pass filter time constant $T_{lpf,b}$ (Figures 8b and 10c), but rather it seems that a low rated power is better from the BESS point of view (Figure 10c). In the best case, 1 h of operation consumes 4.48×10^{-5} h of BESS life (2, 1.5) MW, whereas in the worst case 1.67×10^{-4} h (5, 5) MW. The preferred combination for the PSHP, (4.5, 4) MW, has an associated BESS life consumption equal to 1.034×10^{-4} h.

One would expect LC_b and the BESS power rating to be inversely proportional because increasing the rated power means an increase in energy capacity (as the energy to power ratio is fixed), hence the amplitude of the SOC cycles should be smaller. However what can be seen from Figure 10c is that LC_b tends to increase with the BESS power. This behaviour is explained by the low-pass filter time constant: the higher the power rating the higher the intentional delay. This delay reduces the BESS power fluctuations, but at the same time the power is "slower" in being adjusted, as seen in Figure 11b. Given these findings, we ran a set of simulations with $T_{lpf,b} = 0$, to verify that this is actually beneficial for the BESS. The resulting LC_b was considered the "reference", and the ratio between the LC_b with and without the delay is shown in Figure 10d. It is always convenient to have a non-zero low-pass filter time constant, and the lower the BESS power rating, the more beneficial the delay.

In fixed-speed operation, the non-hybridized turbine wicket gate covers a distance of 0.7150 p.u. with a total of 114 movements. With the (0.5, 0.5) MW configuration, Lwg becomes 75.41 % of the reference value (0.5391 p.u., the maximum in the hybrid configuration), whereas the minimum value is achieved for the combination (5, 4.5) MW (47.30 %, 0.3382 p.u.). The maximum reduction of Nwg (18.42 % of the reference value) is achieved by 3 configurations, the most preferable one (in terms of minimal Lwg) being (5, 4.5) MW.

The fixed-speed results are smaller both in magnitude and in improvement w.r.t. the variable-speed counterpart, as the latter ability to quickly deliver electrical power generates a rotational speed imbalance that requires a stronger action by the speed governor. Being faster in delivering electrical power, the variable-speed admissible intentional delay is higher than the fixed-speed, hence the latter Lwg and Nwg improvements are inferior, in percentage (Figure 12).

Regarding the BESS, the maximum LC_b is experienced with minimal installed powers, (0.5, 0.5) MW: 2.205×10^{-4} h; on the other hand, the minimum life consumption is achieved in the (2.5, 2) MW: 5.09×10^{-5} h. The simulations of the hybrid configurations with $T_{lpf,b} = 0$ confirm that the intentional delay reduces the life consumption of the device. The plot has been omitted as it does not provide additional information w. r. t. Figure 10d.

From the results examined so far, the hybridization of a PSHP emerges as a viable option to meaningfully reduce the wear and tear indicators in a turbine. It is also clear that the best combination of hybridizing powers for the PSHP are not optimal for the BESS in terms of life consumption (which, regardless of the analysed configuration, is always within an acceptable range). Moreover, the presence of a FESS allows for the BESS psp to be filtered from its high frequency components, drastically reducing its cycling and therefore its life consumption.

In pump mode, the torque MWFI decreases at least by about two thirds w.r.t the non-hybridized case (Figure 13a). The fluctuation index was applied to the dimensional torque (kN), sampled every 1 s, to avoid the numerical fluctuations due to the small simulation step size affecting the outcome. The dimensional torque was employed as the MWFI calculation is non-linear, hence the per-unit notation would be inadequate to describe the phenomenon. The index reduction is mostly caused by the rotation angle component θ_i of

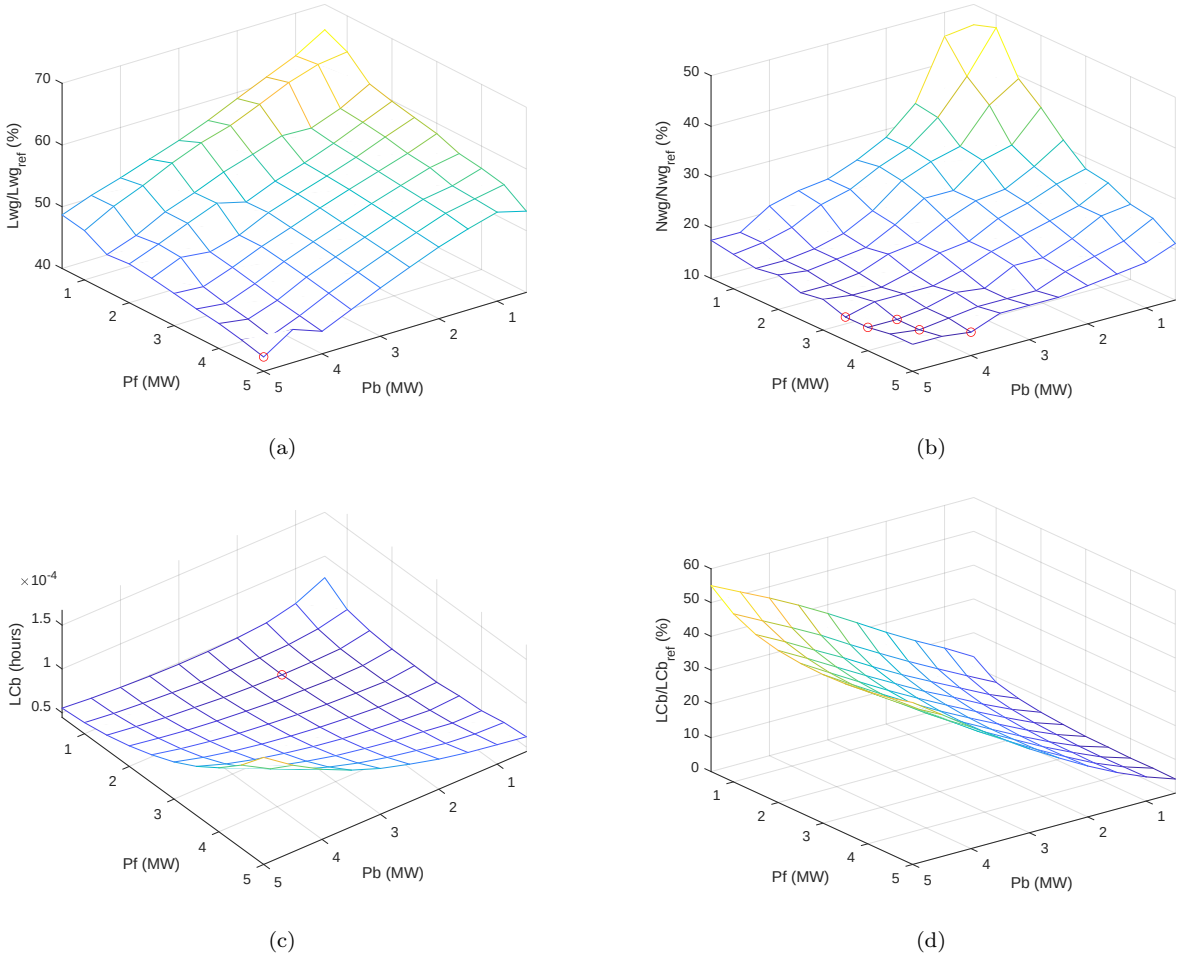

Figure 10: Results for the variable-speed turbine: relative wicket gate travelled distance (a) and number of movements (b), BESS absolute (c) and relative (d) life consumption. $Lwg_{ref} = 0.7564$ p.u., $Nwg_{ref} = 137$.

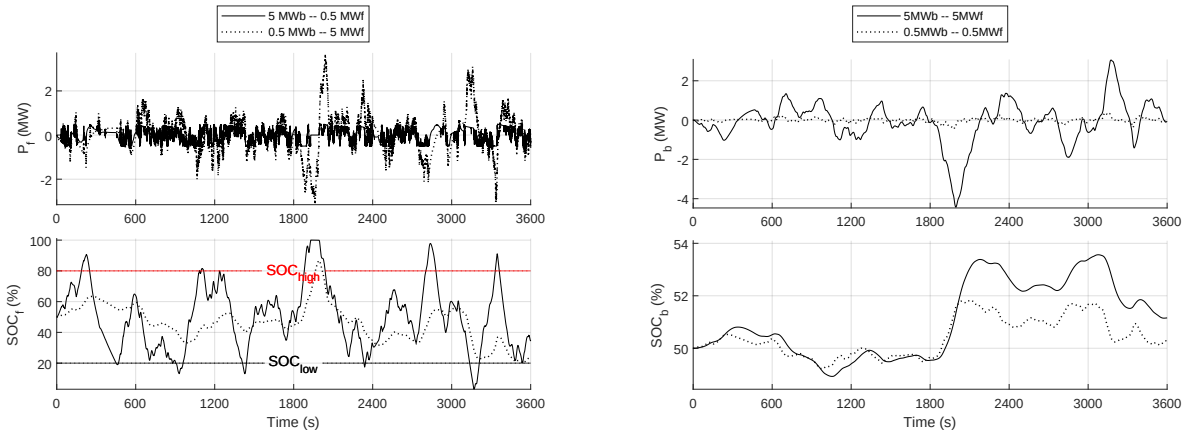

(a) (b)

Figure 11: Comparison between the electric power (top) and SOC (bottom) of FESS (a) and BESS (b) in different configurations. (a) comparison between the configurations (5, 0.5) MW and (0.5, 5) MW. (b) comparison between the configuration (5 5) MW and (0.5, 0.5) MW.

(20), which can be seen from Figure 13b and more clearly in the detail. The MWFI ranges from 12.34 % (4.5, 5) MW of the reference value to 31.05 % (0.5 MW BESS – 0.5 MW FESS).

Finally, we present the comparison between the non-hybrid variable-speed and the hybrid fixed-speed turbines (Figure 14). The variable-speed turbine can properly track the frequency error by itself, and it is clear from Figure 14a that both plants' FCR and FRR are equivalent (obviously the hybrid plant rated power is greater, which entails more power to be delivered to the grid). The main difference is in the PSHP electric power output, and wicket gate movements: the variable-speed operation entails a high number of low-amplitude movements of the wicket gate (Figure 14b), which are eliminated by the action of BESS and FESS. The variable (hybrid fixed) speed wicket gate covers a distance of 0.7563 p.u. (0.3656 p.u.) for a total of 137 (21) movements. On the other hand, the variable-speed technology can provide ancillary services even in pump mode. The BESS and FESS can also provide FCR and FRR in fixed-speed pumping, but they are limited by their rated powers and by the fact that the PSHP cannot control their SOC.

6. Discussion of results

This paper analyses the potential benefits of the hybridization of a seawater PSHP, that would be installed in the island of Sardinia to improve the stability of the electric system (by delivering FCR and FRR) and allow higher permeation of non-programmable RES. According to the pre-feasibility and feasibility studies the PSHP would be equipped with a variable-speed reversible pump-turbine. The industry tends to consider the adoption of the variable-speed technology as an alternative to the hybridization of the PSHP, hence the fixed-speed turbine and its hybridization was included in the study. The fixed-speed pump cannot perform ancillary services, therefore its study was neglected.

A detailed dynamic model of the PSHP was realized in the MATLAB/Simulink environment, including the upper reservoir (assumed at constant geodetic level), penstock, pump-turbine, speed governor, and DFIG (a simplified synchronous generator) model for the variable (fixed) speed operation respectively. The characteristic curves of the pump-turbine were reconstructed via polynomial interpolation from experimental data. The polynomial coefficients were found via a constrained optimization problem, the objective function (to minimize) being the sum of the square errors, subject to a concavity constraint. The model of the BESS coincides with the model of its power converter, as it was assumed that the electrochemical phenomena to be at least one order of magnitude faster than the converter phenomena. A detailed model of a FESS, model "ACEBO", provided by CIEMAT (Madrid, Spain) was included.

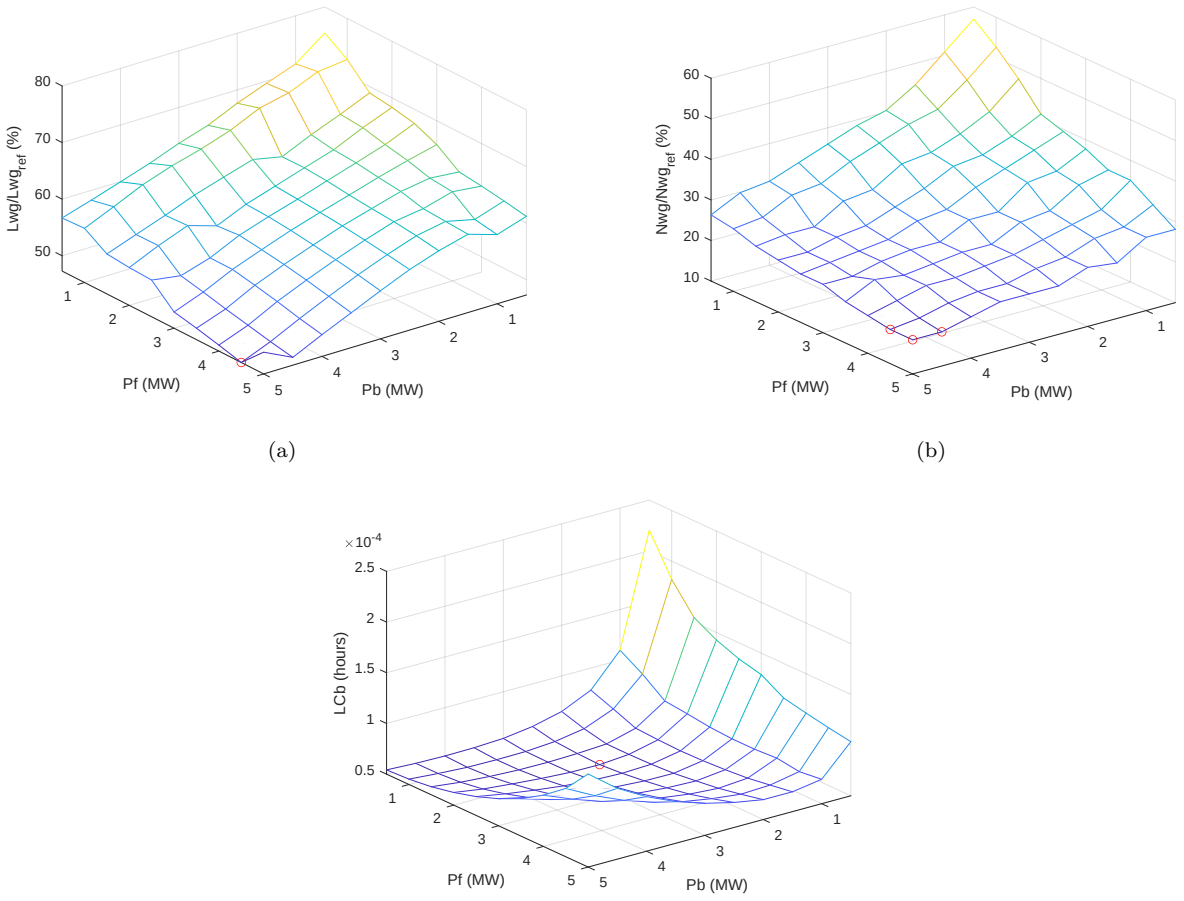

(a) (b)

(c)

Figure 12: Results for the fixed-speed turbine. In the non-hybridized plant (reference case): $Lwg_{ref} = 0.7313$ p.u., $Nwg_{ref} = 122$.

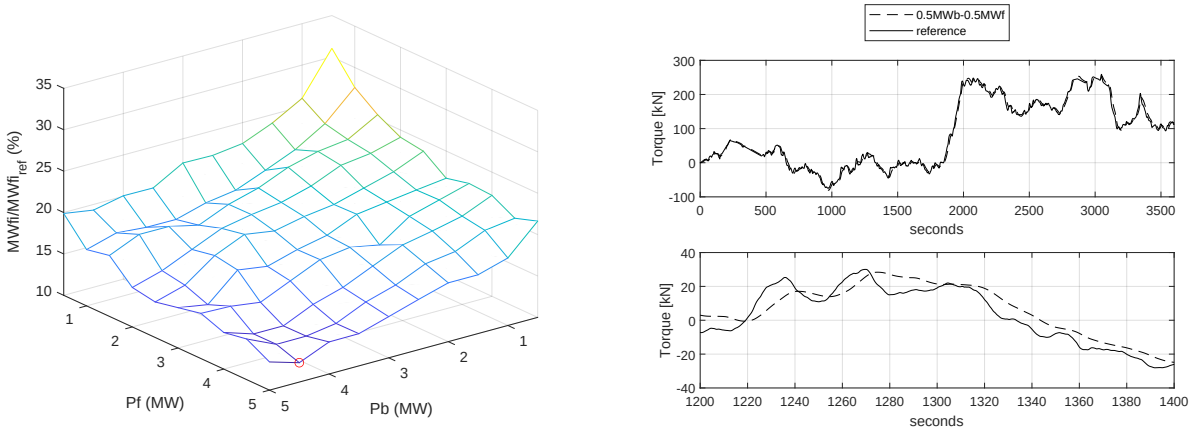

(a) (b)

Figure 13: Results for the variable-speed pump. (a) Mei-Wang fluctuation index of the torque at the shaft (reference case: $MWFi_{ref} = 0.0106$); (b) comparison of the torque between the (non-hybridized) reference case and the plant hybridized with 5 MW of BESS and FESS (top) and detail (bottom).

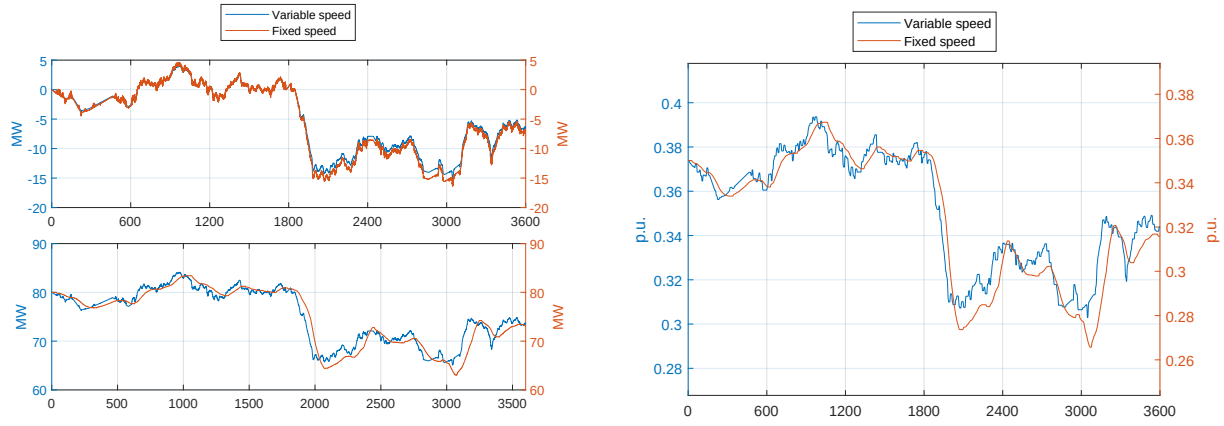

(a) (b)

Figure 14: Comparison between the non-hybrid variable-speed turbine and the hybridized (5 MW of both BESS and FESS) fixed-speed turbine. (a) power plant (top) and PSHP (bottom) electric power output. (b) wicket gate position.

To coordinate the power flows of each technology (hydro, BESS and FESS), a control strategy was developed. The control strategy uses low-pass filters to split the regulation effort into the different technologies: the PSHP is tasked to deal with the lowest frequencies, the BESS with the intermediate, and the FESS with the fastest. Moreover, the PSHP is tasked to perform SOC control of both devices, given its high power rating and energy availability.

For the turbine, the efficacy of the hybridization (in terms of reduction of the wear and tear) was evaluated by calculating the total distance travelled by the wicket gate blades and the number of movements. Due to the lack of an established procedure to perform a similar estimate in pump mode, we proposed to quantify the fluctuations (with the Mei-Wang fluctuation index) of the mechanical torque at the shaft of the pump, assuming it correlates positively with the mechanical stress at the runner and stator.

The BESS life consumption was estimated to be only due to cycling. The number and types of cycles were identified with the Rainflow algorithm applied to the SOC signal, and Miner rule for mechanical fatigue was used to estimate the total life (capacity) loss.

A total of 100 combinations of BESS and FESS power ratings were analysed in the hybrid configurations, from 0.5 MW to 5 MW. The reference configuration was the non-hybridized PSHP (variable-speed pump-turbine and fixed-speed turbine).

The control strategy was calibrated for each combination of BESS and FESS powers by feeding a 200 mHz frequency error step signal to the plant and finding the highest values of the PSHP and BESS low-pass filters' time constants that would respect the TSO's guidelines (50 % of the FCR to be delivered within 15 s, 100 % within 30 s). The higher the power rating of the hybridizing technologies, the more the PSHP and BESS can be slowed (higher low-pass filter time constant). The obtained values for the variable-speed turbine and pump are identical. The calibration process did not involve the SOC control routine.

The plant was simulated open-loop due to the lack of a detailed model of the Sardinian power grid. Real historical frequency and AGC signal from continental Italy were used to simulate the plant performance for 3600 s. During that hour, the most intense frequency error of the day was recorded: about 150 mHz in overfrequency.

The simulations show a consistent decrease in the wear and tear indicators (Lwg and Nwg for the variable/fixed-speed turbine, the shaft torque MWFI for the pump) along with the increase of the BESS and FESS power ratings and the PSHP low-pass filter time constant.

With respect to the reference (non hybridized) case, the turbine Lwg ranges from 42.33 % (0.3202 p.u.) to 65.86 % (0.4984 p.u.) in variable-speed, while in fixed-speed from 47.30 % (0.3382 p.u.) to 75.41 % (0.5391 p.u.). The variable-speed Nwg ranges from 14.60 % (20) to 45.99 % (63), while the fixed-speed from 18.42 % (21) to 57.02 % (65). The variable-speed is more flexible in adjusting its electric power, but this comes at the cost of more and more intense movements of the guide vanes. For this reason, the indicators' reduction for the variable-speed turbine is greater.

The installed BESS and FESS affect the PSHP differently: due to its low energy density the FESS often triggers the SOC control routine. The lower its power rating the more the routine is triggered, but in case of small FESS size the PSHP power adjustment is also low. On the other hand, a high FESS power triggers the SOC control just once, but this requires a more intense action by the PSHP, affecting the guide vanes.

From the BESS point of view, the life consumption does not correlate with its filter time constant, and the results for the variable-speed turbine and pump coincide. High BESS and low FESS powers, and vice versa, are better for the former life consumption, in variable speed, whereas in fixed-speed low FESS powers tend to give better results. In pump mode, the torque fluctuations strongly decrease to 31.05 % of the non-hybridized case even with 0.5 MW of installed power. This does not necessarily imply that the hybridization can benefit the variable-speed pump wear and tear by that much, but it shows that a large part of fluctuations (and therefore pressure waves) are avoided thanks to the coordinated action of BESS and FESS. This is a first attempt to establish a quantitative method to assess the impact of operation of a variable-speed pump via system-wide simulations, without detailed CFD analyses. More studies and experimental data are necessary to improve the models and validate the results of the simulations.

By comparing the electrical power outputs of the non-hybrid variable-speed turbine and its hybrid fixed-speed counterpart, it can be observed that the former is very fast in following the frequency error, but

this comes at the cost of high number of small-amplitude movements of the wicket gate. On the other hand, the hybrid system outcome is comparable thanks to the rapidity of the FESS and BESS. The variable-speed technology could be sufficient by itself from the electric grid point of view, but the plant owner might find the hybridization convenient in terms of reduction of the equipment wear and tear. Moreover, in case of extreme events, the transient imbalance between electrical and mechanical powers of the variable-speed pump-turbine may lead to its rotational speed to reach values outside of the admissible range, effect that can be damped by the installed hybridizing technologies. Eventually, the variable-speed PSHP can provide ancillary services even in pump mode, where the fixed-speed counterpart could do the same only thanks to the hybridization, but limited to the power rating of the BESS and FESS, and with the impossibility to control their SOC.

7. Conclusions

This work has shown that the hybridization of a PSHP results in the decrease of all the wear indicators accounted for. This is true for each and every hybrid configuration considered, with Lwg decreasing to 75.41 % (in the worst case) to 42.33 % of the non-hybrid case, and Nwg between 56.03 % to 14.60 %. We also have shown that the reduction in the pump-turbine wear indicators is greater for a variable-speed unit, compared to the fixed-speed counterpart: the increase in flexibility and system responsiveness comes at the price of more hydro-mechanical stress. At the same time, it was found that the hybridization with BESS and FESS is convenient for the former ageing process, which is reduced by at least 45 %, thanks to the latter handling of the high frequency components of the primary regulation, but the best solution for preserving the BESS does not coincide with the one for preserving the PSHP. All this considered, a good trade-off for the plant owner would be to size the BESS and FESS for the maximum BESS duration, (2, 1.5) MW of BESS and FESS respectively, as it requires less installed power (and capital investment) than the configuration for minimum PSHP wear: (5, 4.5) MW. It should also be remarked that these findings were found by simulating a real hour in the Italian continent, whereas for different case studies the analysis could lead to different outcomes. Eventually, hybridization is well suited for enhancing existing fixed-speed plants (as it was found that the benefic impact is comparable for both fixed and variable-speed machines), such that they could exhibit the same performances as a non-hybrid variable-speed PSHP, from the grid point of view, bearing in mind that a fixed-speed pump (in binary configuration) cannot adjust its power intake to control the SOC of the auxiliaries (BESS and FESS).

Acknowledgements

This work has been financed by the Research Fund for the Italian Electrical System in compliance with the Decree of the Minister of Economic Development April 16, 2018, the European Energy Research Alliance (EERA) JP ES Mobility Scheme, and the Spanish Ministry of Science and Innovation under the grant TED2021-132794B-C21.

List of symbols

Accents		
	The quantity is in per-unit, system base	$\bar{}$
	The quantity is in absolute value.	$\hat{}$
Greek letters		
	Wicket gate position, (°)	α
	Penstock roughness coefficient, 0.3 mm	ϵ
	Battery round-trip efficiency, 0.9	η_b
	Efficiency, (p.u.)	η
	Flow number, (p.u.)	ϕ

	Pressure number, (p.u.)	ψ
	Permanent droop of the plant 0.04 p.u.	σ
	Base wicket gate opening, 33.7°	α^b
	Base hydraulic efficiency, 0.7965	η^b
	Base flow number, 0.1732	ϕ^b
	Base pressure number, 0.4506	ψ^b
Roman letters		
	Base value of the head, 355.5325 m	$\hat{H}^b$
	Base rotational speed, 525 rpm	N_h^b
	Base value of the flowrate, 49.0012 m^3/s	$\hat{Q}^b$
	Flywheel characteristic curve polynomial coefficients, (p.u.)	a_i
	Penstock wave speed, 1000 m/s	a_p
	Conduit cross sectional area, 7.0686 m^2	A
	Turbine' characteristic curves polynomial coefficients, (p.u.)	c_{ij}, d_{ij}
	Depth of charge/discharge cycles	cd
	Electromagnetic torque. $c_{em,min} = 0$ p.u., $c_{em,max} = 1.2$ p.u.	c_{em}
	Charge intensity (p.u.)	ci
	Battery capacity lost	C_{loss}
	Control Signal	CS
	Pump characteristic curves polynomial coefficients, (p.u.)	e_i, f_i
	Battery energy/power ratio, 1 h	EP_{ratio}
	Grid frequency (p.u.)	f
	Friction coefficient 0.0323 p.u.	f_p
	Gravitational acceleration 9.8066 m/s^2	g
	Hydraulic head (p.u.)	h
	Flywheel moment of inertia, 15.50 kg m^2	I
	Turbine governor integral gain, $k_{i,var} = 0.18$, $k_{p,fix} = 4.32$	k_i
	Turbine governor proportional gain, $k_{p,var} = 1.8$, $k_{p,fix} = 2$	k_p
	Length of the conduit, 770 m	L
	Battery life consumption	LC
	Control signal from the Automatic Generation Control (%)	$L_{\%}$
	Travelled distance by the wicket gate blades	Lwg
	Unit rotational speed, (p.u.)	n_{11}
	Number of charge/discharge cycles	nc
	Number of cycles leading to the battery end of life	nf
	Flywheel maximum (base) rotational speed, 9000 rpm	$N_{f,max}$
	Number of finite elements in the penstock discretization, 3	n_{ge}
	Number of movements of the wicket gate blades	Nwg
	Electric power	P
	Power at the rotor. $p_{r,min} = -0.15$ p.u., $p_{r,min} = 0.15$ p.u.	p_r

	Flowrate (p.u.)	q
	Unit flow discharge, (p.u.)	q_{11}
	Flywheel base torque, 26.5258 N m	T^b
	Battery converter time constant, 0.3 s	T_{cB}
	Grid Side Converter time constant, 0.5 s	T_{cH}
	Battery converter delay, 0.1 s	$T_{del,b}$
	Flywheel converter delay, 0.1 s	$T_{del,f}$
	Variable-speed pump/turbine synthetic inertia derivative gain, 0.1 s	T_d
	Variable-speed pump/turbine synthetic noise filter time constant, 2 s	T_{fnf}
	Flywheel self-discharge losses, 0.07 N m	T_{loss}
	Doubly Fed Induction Generator mechanical starting time, 6 s	T_m
	Speed governor servomotor time constant, 0.5 s	T_s
	Hydraulic starting time 1.5310 s	T_w
Subscripts		
	Average	avg
	Battery Energy Storage System	b
	Rated power of the power plant.	eff
	Flywheel Energy Storage System	f
	Hydro power plant	h
	i-th element	i
	Primary regulation	I
	Secondary regulation	II
	j-th element	j
	k-th element	k
	Low-pass filter	lpf
	Mechanical	$mech$
	Pump	p
	Synchronous	syn
	Turbine	t
Superscripts		
	Value at $t = 0$	0
	Base quantity	b
	Lower	L
	Related to the State of Charge	SOC
	Upper	U

Acronyms

AGC	Automatic Generation Control
BESS	Battery Energy Storage System
CFD	Computational Fluid Dynamics
DFIG	Doubly Fed Induction Generator
FCR	Frequency Containment Reserve
FESS	Flywheel Energy Storage System
FRR	Frequency Restoration Reserve
GSC	Grid Side Converter

HESS	Hybrid Energy Storage System
m.b.	machine-base
MWFI	Mei-Wang Fluctuation Index
PI	Proportional Integral
PSHP	Pumped Storage Hydro Power
psp	power set-point
PV	photovoltaic
RES	Renewable Energy Sources
RSC	Rotor Side Converter
s.b.	system-base
SC	supercapacitor
SOC	State Of Charge
TSO	Transmission System Operator
WTG	Wind Turbine Generator

References

[1] IEA. Renewables Information: Overview. Technical report, International Energy Agency, Paris, 2020. URL https://www.iea.org/reports/renewables-information-overview.

[2] Wilhelm Winter. European Wind Integration Study (EWIS). Towards a successful integration of large scale wind power into European electricity grids. Final report, 2010.

[3] EPRI. Electric Energy Storage Technology Options: A White Paper Primer on Applications, Costs and Benefits. *EPRI*, pages 1–170, 2010. URL http://large.stanford.edu/courses/2012/ph240/doshay1/docs/EPRI.pdf.

[4] Oliver Schmidt, Sylvain Melchior, Adam Hawkes, and Iain Staffell. Projecting the Future Levelized Cost of Electricity Storage Technologies. *Joule*, 3(1):81–100, January 2019. ISSN 25424351. doi: 10.1016/j.joule.2018.12.008.

[5] G. Ardizzon, G. Cavazzini, and G. Pavesi. A new generation of small hydro and pumped-hydro power plants: Advances and future challenges. *Renewable and Sustainable Energy Reviews*, 31:746–761, March 2014. ISSN 1364-0321. doi: 10.1016/j.rser.2013.12.043. URL http://www.sciencedirect.com/science/article/pii/S1364032113008575.

[6] Giovanna Cavazzini, Juan I. Pérez-Díaz, Francisco Blázquez, Carlos Platero, Jesús Fraile-Ardanuy, José A. Sánchez, and Manuel Chazarra. Pumped-storage hydropower plants: The new generation. In *Energy Storage*, pages 27–80. World Scientific, June 2017. doi: 10.1142/9789813208964_0002. URL https://doi.org/10.1142/9789813208964_0002.

[7] Edson Bortoni, Zulcy de Souza, Augusto Viana, Helcio Villa-Nova, Ângelo Rezek, Luciano Pinto, Roberto Siniscalchi, Rafael Bragança, and José Bernardes. The Benefits of Variable Speed Operation in Hydropower Plants Driven by Francis Turbines. *Energies*, 12(19):3719, January 2019. doi: 10.3390/en12193719. URL https://www.mdpi.com/1996-1073/12/19/3719.

[8] Igor Iliev, Chirag Trivedi, and Ole Gunnar Dahlhaug. Variable-speed operation of Francis turbines: A review of the perspectives and challenges. *Renewable and Sustainable Energy Reviews*, 103(7491):109–121, 2019. doi: 10.1016/j.rser.2018.12.033. URL https://doi.org/10.1016/j.rser.2018.12.033.

[9] Johan Morren, Jan Pierik, and Sjoerd W.H. de Haan. Inertial response of variable speed wind turbines. *Electric Power Systems Research*, 76(11):980–987, July 2006. doi: 10.1016/j.epsr.2005.12.002. URL https://doi.org/10.1016/j.epsr.2005.12.002.

[10] Ioannis D. Margaris, Stavros A. Papathanassiou, Nikos D. Hatziargyriou, Anca D. Hansen, and Poul Sorensen. Frequency control in autonomous power systems with high wind power penetration. *IEEE Transactions on Sustainable Energy*, 3(2):189–199, April 2012. doi: 10.1109/tste.2011.2174660. URL https://doi.org/10.1109/tste.2011.2174660.

[11] Jiri Koutnik. Hydro Power Plants. *AGCS Expert Days 2013, Munich*, 2013. doi: 10.0000/scribd.com/310381055.

[12] Juan Ignacio Pérez-Díaz, Giovanna Cavazzini, F. Blázquez, C Platero, J. Fraile-Ardanuy, José Ángel Sánchez-Fernández, and M Chazarra. Technological developments for pumped-hydro energy storage, Technical Report, Mechanical Storage Subprogramme, Joint Programme on Energy Storage. Technical report, European Energy Research Alliance, 2014.

[13] REN21. Renewables 2021 Global Status Report. Technical report, REN21 Secretariat, Paris, 2021.

[14] Alexandre Oudalov, Daniel Chartouni, and Christian Ohler. Optimizing a battery energy storage system for primary frequency control. *IEEE Transactions on Power Systems*, 22(3):1259–1266, August 2007. doi: 10.1109/tpwrs.2007.901459. URL https://doi.org/10.1109/tpwrs.2007.901459.

[15] Rahul Walawalkar, Jay Apt, and Rick Mancini. Economics of electric energy storage for energy arbitrage and regulation in New York. *Energy Policy*, 35(4):2558–2568, April 2007. ISSN 0301-4215. doi: 10.1016/j.enpol.2006.09.005. URL http://www.sciencedirect.com/science/article/pii/S0301421506003545.

[16] M. Benini, S. Canevese, D. Cirio, and A. Gatti. Battery energy storage systems for the provision of primary and secondary frequency regulation in Italy. In *2016 IEEE 16th International Conference on Environment and Electrical Engineering (EEEIC)*, pages 1–6, Florence, Italy, June 2016. IEEE. ISBN 978-1-5090-2320-2. doi: 10.1109/EEEIC.2016.7555748. URL http://ieeexplore.ieee.org/document/7555748/.

[17] Holger Hesse, Michael Schimpe, Daniel Kucevic, and Andreas Jossen. Lithium-Ion Battery Storage for the Grid—A Review of Stationary Battery Storage System Design Tailored for Applications in Modern Power Grids. *Energies*, 10(12):2107, December 2017. ISSN 1996-1073. doi: 10.3390/en10122107.

[18] Tomi Makinen, Aki Leinonen, and Markus Ovaskainen. Modelling and benefits of combined operation of hydropower unit and battery energy storage system on grid primary frequency control. In *2020 IEEE International Conference on Environment and Electrical Engineering and 2020 IEEE Industrial and Commercial Power Systems Europe (EEEIC / I&CPS Europe)*, pages 1–6, Madrid, Spain, June 2020. IEEE. ISBN 978-1-72817-455-6. doi: 10.1109/EEEIC/ICPSEurope49358.2020.9160666.

[19] Jonas Engels, Bert Claessens, and Geert Deconinck. Combined Stochastic Optimization of Frequency Control and Self-Consumption With a Battery. *IEEE Transactions on Smart Grid*, 10(2):1971–1981, March 2019. ISSN 1949-3053, 1949-3061. doi: 10.1109/TSG.2017.2785040.

[20] M. Sufyan, N. A. Rahim, M. M. Aman, C. K. Tan, and S. R. S. Raihan. Sizing and applications of battery energy storage technologies in smart grid system: A review. *Journal of Renewable and Sustainable Energy*, 11(1):014105, January 2019. ISSN 1941-7012. doi: 10.1063/1.5063866.

[21] Jan Figgener, Peter Stenzel, Kai-Philipp Kairies, Jochen Linßen, David Haberschusz, Oliver Wessels, Martin Robinius, Detlef Stolten, and Dirk Uwe Sauer. The development of stationary battery storage systems in Germany – status 2020. *Journal of Energy Storage*, 33:101982, January 2021. ISSN 2352152X. doi: 10.1016/j.est.2020.101982.

[22] Jun Hou, Ziyou Song, Heath F. Hofmann, and Jing Sun. Control Strategy for Battery/Flywheel Hybrid Energy Storage in Electric Shipboard Microgrids. *IEEE Transactions on Industrial Informatics*, 17(2):1089–1099, February 2021. ISSN 1551-3203, 1941-0050. doi: 10.1109/TII.2020.2973409.

[23] Gaojun Meng, Qingqing Chang, Yukun Sun, Yufei Rao, Feng Zhang, Yao Wu, and Ling Su. Energy Storage Auxiliary Frequency Modulation Control Strategy Considering ACE and SOC of Energy Storage. *IEEE Access*, 9:26271–26277, 2021. ISSN 2169-3536. doi: 10.1109/ACCESS.2021.3058146.

[24] Tjark Thien, Hendrik Axelsen, Michael Merten, and Dirk Uwe Sauer. Energy management of stationary hybrid battery energy storage systems using the example of a real-world 5 MW hybrid battery storage project in Germany. *Journal of Energy Storage*, 51:104257, July 2022. ISSN 2352152X. doi: 10.1016/j.est.2022.104257.

[25] Xiaomin Wu, Shaoyi Li, Shengfeng Gan, and Changhui Hou. An Adaptive Energy Optimization Method of Hybrid Battery-Supercapacitor Storage System for Uncertain Demand. *Energies*, 15(5):1765, February 2022. ISSN 1996-1073. doi: 10.3390/en15051765.

[26] Ioannis Hadjipaschalis, Andreas Poullikkas, and Venizelos Efthimiou. Overview of current and future energy storage technologies for electric power applications. *Renewable and Sustainable Energy Reviews*, 13(6-7):1513–1522, August 2009. doi: 10.1016/j.rser.2008.09.028. URL `https://doi.org/10.1016/j.rser.2008.09.028`.

[27] K.C. Divya and Jacob Østergaard. Battery energy storage technology for power systems—an overview. *Electric Power Systems Research*, 79(4):511–520, April 2009. doi: 10.1016/j.epsr.2008.09.017. URL `https://doi.org/10.1016/j.epsr.2008.09.017`.

[28] Furquan Nadeem, S. M. Suhail Hussain, Prashant Kumar Tiwari, Arup Kumar Goswami, and Taha Selim Ustun. Comparative Review of Energy Storage Systems, Their Roles, and Impacts on Future Power Systems. *IEEE Access*, 7:4555–4585, 2019. ISSN 2169-3536. doi: 10.1109/ACCESS.2018.2888497.

[29] Micah S. Ziegler and Jessika E. Trancik. Re-examining rates of lithium-ion battery technology improvement and cost decline. *Energy & Environmental Science*, 14(4):1635–1651, 2021. ISSN 1754-5692, 1754-5706. doi: 10.1039/D0EE02681F.

[30] Jisung Lee, Sangkwon Jeong, Y.H. Han, and Byung Park. Concept of Cold Energy Storage for Superconducting Flywheel Energy Storage System. *IEEE Transactions on Applied Superconductivity*, 21:2221–2224, June 2011. doi: 10.1109/TASC.2010.2094177.

[31] M. L. Lazarewicz and A. Rojas. Grid frequency regulation by recycling electrical energy in flywheels. In *IEEE Power Engineering Society General Meeting, 2004.*, pages 2038–2042 Vol.2, 2004. doi: 10.1109/PES.2004.1373235.

[32] A. Buchroithner, A. Haan, R. Pressmair, M. Bader, B. Schweighofer, H. Wegleiter, and H. Edtmayer. Decentralized low-cost flywheel energy storage for photovoltaic systems. In *2016 International Conference on Sustainable Energy Engineering and Application (ICSEEA)*. IEEE, October 2016. doi: 10.1109/icseea.2016.7873565. URL `https://doi.org/10.1109/icseea.2016.7873565`.

[33] Mustafa Amiryar and Keith Pullen. A review of flywheel energy storage system technologies and their applications. *Applied Sciences*, 7(3):286, March 2017. doi: 10.3390/app7030286. URL `https://doi.org/10.3390/app7030286`.

[34] Franziska Goris and Eric L. Severson. A review of flywheel energy storage systems for grid application. In *IECON 2018 - 44th Annual Conference of the IEEE Industrial Electronics Society*. IEEE, October 2018. doi: 10.1109/iecon.2018.8591842. URL `https://doi.org/10.1109/iecon.2018.8591842`.

[35] Umer Akram, Mithulananthan Nadarajah, Rakibuzzaman Shah, and Federico Milano. A review on rapid responsive energy storage technologies for frequency regulation in modern power systems. *Renewable and Sustainable Energy Reviews*, 120:109626, March 2020. doi: 10.1016/j.rser.2019.109626. URL `https://doi.org/10.1016/j.rser.2019.109626`.

[36] Subhashree Choudhury. Flywheel energy storage systems: A critical review on technologies, applications, and future prospects. *International Transactions on Electrical Energy Systems*, 31(9), July 2021. doi: 10.1002/2050-7038.13024. URL https://doi.org/10.1002/2050-7038.13024.

[37] Iman Naziri Moghaddam and Badrul Chowdhury. Optimal sizing of Hybrid Energy Storage Systems to mitigate wind power fluctuations. *IEEE Power and Energy Society General Meeting*, 2016-November: 1–5, 2016. doi: 10.1109/PESGM.2016.7741862.

[38] Mohammed Guezgouz, Jakub Jurasz, Bennaissa Bekkouche, Tao Ma, Muhammad Shahzad Javed, and Alexander Kies. Optimal hybrid pumped hydro-battery storage scheme for off-grid renewable energy systems. *Energy Conversion and Management*, 199:112046, November 2019. doi: 10.1016/j.enconman.2019.112046. URL https://doi.org/10.1016/j.enconman.2019.112046.

[39] Yoga Anindito, Jannik Haas, Marcelo Olivares, Wolfgang Nowak, and Jordan Kern. A new solution to mitigate hydropeaking? batteries versus re-regulation reservoirs. *Journal of Cleaner Production*, 210:477–489, February 2019. doi: 10.1016/j.jclepro.2018.11.040. URL https://doi.org/10.1016/j.jclepro.2018.11.040.

[40] David Valentín, Alexandre Presas, Mònica Egusquiza, Jean-Louis Drommi, and Carme Valero. Benefits of battery hybridization in hydraulic turbines. Wear and tear evaluation in a Kaplan prototype. *Renewable Energy*, 199:35–43, November 2022. ISSN 09601481. doi: 10.1016/j.renene.2022.08.117.

[41] Yuri V. Makarov, Bo Yang, John G. DeSteese, Shuai Lu, Carl H. Miller, Preben Nyeng, Jian Ma, Donald J. Hammerstrom, and Vilanyur V. Vishwanathan. Wide-area energy storage and management system to balance intermittent resources in the bonneville power administration and california ISO control areas. Technical report, June 2008. URL https://doi.org/10.2172/947483.

[42] Ning Lu, Yuri V. Makarov, Mark R. Weimar, Frank Rudolph, Shashikala Murthy, Jim Arseneaux, Clyde Loutan, and S. Chowdhury. THE WIDE-AREA ENERGY STORAGE AND MANAGEMENT SYSTEM PHASE II final report - flywheel field tests. Technical report, August 2010. URL https://doi.org/10.2172/991592.

[43] José Ignacio Sarasua, Guillermo Martínez-Lucas, Hilel García-Pereira, Gustavo Navarro-Soriano, Ángel Molina-García, and Ana Fernández-Guillamón. Hybrid frequency control strategies based on hydropower, wind, and energy storage systems: Application to 100% renewable scenarios. *IET Renewable Power Generation*, 16(6):1107–1120, April 2022. ISSN 1752-1416, 1752-1424. doi: 10.1049/rpg2.12326.

[44] Dong Jing Lee and Li Wang. Small-signal stability analysis of an autonomous hybrid renewable energy power generation/energy storage system part I: Time-domain simulations. *IEEE Transactions on Energy Conversion*, 23(1):311–320, 2008. doi: 10.1109/TEC.2007.914309.

[45] Hansang Lee, Byoung Yoon Shin, Sangchul Han, Seyong Jung, Byungjun Park, and Gilsoo Jang. Compensation for the power fluctuation of the large scale wind farm using hybrid energy storage applications. *IEEE Transactions on Applied Superconductivity*, 22(3):5701904–5701904, 2012. doi: 10.1109/TASC.2011.2180881.

[46] L. Barelli, G. Bidini, F. Bonucci, L. Castellini, A. Fratini, F. Gallorini, and A. Zuccari. Flywheel hybridization to improve battery life in energy storage systems coupled to RES plants. *Energy*, 173: 937–950, 2019. doi: 10.1016/j.energy.2019.02.143. URL https://doi.org/10.1016/j.energy.2019.02.143.

[47] Jorge Torres, Marcos Blanco, Marcos Lafoz, Gustavo Navarro, Jorge Nájera, and Miguel Santos-Herran. Dimensioning Methodology of Energy Storage Systems for Power Smoothing in a Wave Energy Conversion Plant Considering Efficiency Maps and Filtering Control Techniques. *Energies*, 13(13):3380, July 2020. ISSN 1996-1073. doi: 10.3390/en13133380. URL http://dx.doi.org/10.3390/en13133380.

[48] Philipp Glücker, Klaus Kivekäs, Jari Vepsäläinen, Panagiotis Mouratidis, Maximilian Schneider, Stephan Rinderknecht, and Kari Tammi. Prolongation of battery lifetime for electric buses through flywheel integration. *Energies*, 14(4):899, February 2021. doi: 10.3390/en14040899. URL `https://doi.org/10.3390/en14040899`.

[49] Ali Asghar Khodadoost Arani, Gevork B. Gharehpetian, and Mehrdad Abedi. A novel control method based on droop for cooperation of flywheel and battery energy storage systems in islanded microgrids. *IEEE Systems Journal*, 14(1):1080–1087, March 2020. doi: 10.1109/jsyst.2019.2911160. URL `https://doi.org/10.1109/jsyst.2019.2911160`.

[50] T. R. Ayodele, A. S. O. Ogunjuyigbe, and N. O. Oyelowo. Hybridisation of battery/flywheel energy storage system to improve ageing of lead-acid batteries in PV-powered applications. *International Journal of Sustainable Engineering*, 13(5):337–359, September 2020. ISSN 1939-7038, 1939-7046. doi: 10.1080/19397038.2020.1725177.

[51] Pawan Seshadri Venkatesh, Vishnu Chandran, and Sreeram Anil. Study of Flywheel Energy Storage in a Pure EV Powertrain in a Parallel Hybrid Setup and Development of a Novel Flywheel Design for Regeneration Efficiency Improvement. In *SAE WCX Digital Summit*, pages 2021–01–0721, April 2021. doi: 10.4271/2021-01-0721.

[52] Stefan Breban, Mehdi Nasser, Arnaud Vergnol, Benoît Robyns, and Mircea M. Radulescu. Hybrid wind/microhydro power system associated with a supercapacitor energy storage device - Experimental results. *Proceedings of the 2008 International Conference on Electrical Machines, ICEM'08*, pages 1–6, 2008. doi: 10.1109/ICELMACH.2008.4800026.

[53] V. Gevorgian, E. Muljadi, Yusheng Luo, M. Mohanpurkar, R. Hovsapian, and V. Koritarov. Supercapacitor to provide ancillary services. *2017 IEEE Energy Conversion Congress and Exposition, ECCE 2017*, 2017-January(October):1030–1036, 2017. doi: 10.1109/ECCE.2017.8095900.

[54] Wei Li and Géza Joós. A power electronic interface for a battery supercapacitor hybrid energy storage system for wind applications. *PESC Record - IEEE Annual Power Electronics Specialists Conference*, pages 1762–1768, 2008. doi: 10.1109/PESC.2008.4592198.

[55] Wei Li, Géza Joós, and Jean Bélanger. Real-time simulation of a wind turbine generator coupled with a battery supercapacitor energy storage system. *IEEE Transactions on Industrial Electronics*, 57(4): 1137–1145, 2010. doi: 10.1109/TIE.2009.2037103.

[56] Linquan Bai, Fangxing Li, Qinran Hu, Hantao Cui, and Xin Fang. Application of battery-supercapacitor energy storage system for smoothing wind power output: An optimal coordinated control strategy. *IEEE Power and Energy Society General Meeting*, 2016-November:1–5, 2016. doi: 10.1109/PESGM.2016.7741798.

[57] Feng Guo and Ratnesh Sharma. Hybrid Energy Storage Systems integrating battery and Ultracapacitor for the PJM frequency regulation market. *IEEE Power and Energy Society General Meeting*, 2016-November:1–4, 2016. doi: 10.1109/PESGM.2016.7741867.

[58] Stalin Munoz Vaca, Charalampos Patsios, and Phil Taylor. Enhancing frequency response of wind farms using hybrid energy storage systems. *2016 IEEE International Conference on Renewable Energy Research and Applications, ICRERA 2016*, 5:325–329, 2016. doi: 10.1109/ICRERA.2016.7884560.

[59] Umer Akram and Muhammad Khalid. A Coordinated Frequency Regulation Framework Based on Hybrid Battery-Ultracapacitor Energy Storage Technologies. *IEEE Access*, 6:7310–7320, 2017. doi: 10.1109/ACCESS.2017.2786283.

[60] Umer Akram, Muhammad Khalid, and Saifullah Shafiq. An innovative hybrid wind-solar and battery-supercapacitor microgrid system—development and optimization. *IEEE Access*, 5:25897–25912, 2017. doi: 10.1109/ACCESS.2017.2767618.

[61] Younghyun Kim, Vijay Raghunathan, and Anand Raghunathan. Design and Management of Battery-Supercapacitor Hybrid Electrical Energy Storage Systems for Regulation Services. *IEEE Transactions on Multi-Scale Computing Systems*, 3(1):12–24, 2017. doi: 10.1109/TMSCS.2016.2627543.

[62] Stalin Munoz Vaca, Charalampos Patsios, and Phil Taylor. Sizing of hybrid energy storage systems for frequency response of solar farms in Ecuador. *2017 IEEE PES Innovative Smart Grid Technologies Conference - Latin America, ISGT Latin America 2017*, 2017-January:1–7, 2017. doi: 10.1109/ISGT-LA.2017.8126749.

[63] J.C. Hernández, F. Sanchez-Sutil, F.J. Muñoz-Rodríguez, and C.R. Baier. Optimal sizing and management strategy for PV household-prosumers with self-consumption/sufficiency enhancement and provision of frequency containment reserve. *Applied Energy*, 277:115529, November 2020. ISSN 03062619. doi: 10.1016/j.apenergy.2020.115529.

[64] Mohammed Abdulelah Albasheri, Ouahid Bouchhida, Youcef Soufi, Abdelhafidh Moualdia, and Mujammal Mujammal. Control And Power Management of DC Microgrid Based Wind/Battery/Supercapacitor. In *2022 IEEE 2nd International Maghreb Meeting of the Conference on Sciences and Techniques of Automatic Control and Computer Engineering (MI-STA)*, pages 680–685, Sabratha, Libya, May 2022. IEEE. ISBN 978-1-66547-918-9. doi: 10.1109/MI-STA54861.2022.9837665.

[65] Kendall Mongird, Vilayanur Viswanathan, Patrick Balducci, Jan Alam, Vanshika Fotedar, Vladimir Koritarov, and Boualem Hadjerioua. An Evaluation of Energy Storage Cost and Performance Characteristics. *Energies*, 13(13):3307, June 2020. ISSN 1996-1073. doi: 10.3390/en13133307.

[66] Chunlian Jin, Ning Lu, Shuai Lu, Yuri Makarov, and Roger A. Dougal. Coordinated control algorithm for hybrid energy storage systems. *IEEE Power and Energy Society General Meeting*, pages 1–7, 2011. doi: 10.1109/PES.2011.6039893.

[67] Chunlian Jin, Ning Lu, Shuai Lu, Yuri V. Makarov, and Roger A. Dougal. A coordinating algorithm for dispatching regulation services between slow and fast power regulating resources. *IEEE Transactions on Smart Grid*, 5(2):1043–1050, 2014. doi: 10.1109/TSG.2013.2277974.

[68] Danilo Laban. Hydro/Battery Hybrid Systems for Frequency Regulation. Master's thesis, Escola Tècnica Superior d'Enginyria Industrial de Barcelona, 2019.

[69] Quanyuan Jiang and Haisheng Hong. Wavelet-based capacity configuration and coordinated control of hybrid energy storage system for smoothing out wind power fluctuations. *IEEE Transactions on Power Systems*, 28(2):1363–1372, 2013. doi: 10.1109/TPWRS.2012.2212252.

[70] Jingang Han, Jean-Frederic Charpentier, and Tianhao Tang. An energy management system of a fuel cell/battery hybrid boat. *Energies*, 7(5):2799–2820, April 2014. doi: 10.3390/en7052799. URL `https://doi.org/10.3390/en7052799`.

[71] Blanca Torres, Vara José, Ignacio Sarasúa, Moreno Juan, Ignacio Pérez-Díaz, and Marcos Lafoz. Control strategy and sizing of a flywheel energy storage plant for the frequency control of an isolated wind-hydro power system. *15 th Wind Integration Workshop*, November, 2016.

[72] Mutchimas Kheawcum and Somboon Sangwongwanich. A Case Study on Flywheel Energy Storage System Application for Frequency Regulation of Islanded Amphoe Mueang Mae Hong Son Microgrid. In *2020 17th International Conference on Electrical Engineering/Electronics, Computer, Telecommunications and Information Technology (ECTI-CON)*, pages 1–4, Phuket, Thailand, June 2020. IEEE. ISBN 978-1-72816-486-1. doi: 10.1109/ECTI-CON49241.2020.9158108. URL `https://ieeexplore.ieee.org/document/9158108/`.

[73] Terna. Progetto Pilota Servizio di regolazione ultra-rapida di frequenza (" Fast Reserve ") Relazione di accompagnamento. Technical report, TERNA, November 2019.

[74] Massimo Meghella, Julio Alterach, Elena Gobbi, Giacomo Gardini, and Ruggero Marazzi. Studi e analisi di pre-fattibilità per l'integrazione ottimale in rete dell'energia prodotta da fonti rinnovabili mediante sistemi di pompaggio marino. Technical report, Ricerca sul Sistema Energetico, January 2013.

[75] Julio Alterach, Andrea Danelli, Massimo Meghella, Simone Sperati, R Calisti, Antonio Gatti, Ruggero Marazzi, Giuseppe Bruno, Francesco Careri, F Davò, Angelo L'abbate, and Andrea Pitto. Progetto di massima e valutazione tecnico economica di un impianto di pompaggio e generazione marino, mediante l'utilizzo di macchine reversibili a giri variabili. Technical report, Ricerca sul Sistema Energetico, February 2014.

[76] Julio Alterach, Roberto Maurizio Calisti, Maria Vittoria Cazzol, Giuseppe Bruno, Ruggero Marazzi, Angelo L'abbate, Andrea Amicarelli, Andrea Danelli, Francesco Careri, and Simone Sperati. Impianto di pompaggio marino: iniziative per la fattibilità e l'integrazione ottimale in rete. Technical report, Ricerca sul Sistema Energetico, January 2015.

[77] Akitaka Hiratsuka, Takashi Arai, and Tsukasa Yoshimura. Seawater pumped-storage power plant in okinawa island, japan. *Engineering Geology*, 35(3-4):237–246, October 1993. doi: 10.1016/0013-7952(93)90012-2. URL `https://doi.org/10.1016/0013-7952(93)90012-2`.

[78] Katsuhiro Oshima, Juichiro Kawai, Shiro Otsuka, Toshiro Wada, and Haruo Imano. Development of pump-turbine for seawater pumped storage power plant. In *Waterpower '99*. American Society of Civil Engineers, July 1999. doi: 10.1061/40440(1999)67. URL `https://doi.org/10.1061/40440(1999)67`.

[79] Ana Fernández-Guillamón, Eduard Muljadi, and Angel Molina-García. Frequency control studies: A review of power system, conventional and renewable generation unit modeling. *Electric Power Systems Research*, 211:108191, October 2022. ISSN 03787796. doi: 10.1016/j.epsr.2022.108191.

[80] TERNA. L'elettricità nelle regioni. Technical report, TERNA, 2020. URL `https://download.terna.it/terna/9-REGIONI_8d8e25b6ff538b1.pdf`.

[81] Terna. Partecipazione Alla Regolazione Di Frequenza e Frequenza-Potenza. Technical Report Allegato A15, Terna, 2008. URL `https://download.terna.it/terna/0000/0105/32.pdf`.

[82] MATLAB. *version R2020b*. The MathWorks Inc., Natick, Massachusetts, 2020.

[83] M Hanif Chaudhry. *Applied hydraulic transients*. Springer, 1979.

[84] Xianlin Liu and Chu Liu. Eigenanalysis of oscillatory instability of a hydropower plant including water conduit dynamics. *IEEE Transactions on Power Systems*, 22(2):675–681, May 2007. doi: 10.1109/tpwrs.2007.895156. URL `https://doi.org/10.1109/tpwrs.2007.895156`.

[85] José Ignacio Sarasúa, Juan Ignacio Pérez-Díaz, José Román Wilhelmi, and José Ángel Sánchez-Fernández. Dynamic response and governor tuning of a long penstock pumped-storage hydropower plant equipped with a pump-turbine and a doubly fed induction generator. *Energy Conversion and Management*, 106:151–164, December 2015. doi: 10.1016/j.enconman.2015.09.030. URL `https://doi.org/10.1016/j.enconman.2015.09.030`.

[86] Pierangelo Andreini. *Manuale dell'ingegnere meccanico*. Hoepli Editore, 2002.

[87] F. P. de Mello, R. J. Koessler, J. Aaee, P. M. Anderson, J. H. Doudna, J. H. Fish, P. A.L. Hamm, Prabha Kundur, D. C. Lee, G. J. Rogers, and C. Taylor. Hydraulic turbine and turbine control models for system dynamic studies working group on prime mover and energy supply models for system dynamic performance studies. *IEEE Transactions on Power Systems*, 7(1):167–179, 1992. doi: 10.1109/59.141700.

[88] Juan Ignacio Pérez-Díaz, José Ignacio Sarasúa, and José Román Wilhelmi. Contribution of a hydraulic short-circuit pumped-storage power plant to the load-frequency regulation of an isolated power system. *International Journal of Electrical Power and Energy Systems*, 62:199–211, 2014. doi: 10.1016/j.ijepes.2014.04.042.

[89] S. P. Mansoor, D. I. Jones, D. A. Bradley, F. C. Aris, and G. R. Jones. Reproducing oscillatory behaviour of a hydroelectric power station by computer simulation. *Control Engineering Practice*, 8 (11):1261–1272, 2000. doi: 10.1016/S0967-0661(00)00068-X.

[90] German Ardul Munoz-Hernandez, Sa'ad Petrous Mansoor, and Dewi Ieuan Jones. *Modelling and Controlling Hydropower Plants*. Advances in Industrial Control. Springer London, London, 2013. ISBN 978-1-4471-2290-6 978-1-4471-2291-3. doi: 10.1007/978-1-4471-2291-3.

[91] José Ignacio Sarasúa, Juan Ignacio Pérez-Díaz, and Blanca Torres Vara. On the implementation of variable speed in pump-turbine units providing primary and secondary load-frequency control in generating mode. *Energies*, 8(12):13559–13575, 2015. doi: 10.3390/en81212382.

[92] Jan Machowski, Zbigniew Lubosny, Janusz W Bialek, and James R Bumby. *Power system dynamics: stability and control*. John Wiley & Sons, 2020.

[93] Linn Saarinen, Per Norrlund, and Urban Lundin. Field Measurements and System Identification of Three Frequency Controlling Hydropower Plants. *IEEE Transactions on Energy Conversion*, 30 (3):1061–1068, September 2015. ISSN 0885-8969, 1558-0059. doi: 10.1109/TEC.2015.2425915. URL `http://ieeexplore.ieee.org/document/7110341/`.

[94] E. Kopf and S. Brausewetter. Control strategies for variable speed machines - design and optimization criteria. *Hydro*, (figure 1), 2005.

[95] Weijia Yang, Jiandong Yang, Wencheng Guo, Wei Zeng, Chao Wang, Linn Saarinen, and Per Norrlund. A mathematical model and its application for hydro power units under different operating conditions. *Energies*, 8(9):10260–10275, 2015. doi: 10.3390/en80910260.

[96] Jon Are Suul, Kjetil Uhlen, and Tore Undeland. Variable speed pumped storage hydropower for integration of wind energy in isolated grids – case description and control strategies. In *NORPIE/2008, Nordic Workshop on Power and Industrial Electronics, June*, page 8, 2008.

[97] R Bessa, C Moreira, B Silva, J Filipe, and N Fulgêncio. Role of pump hydro in electric power systems. *Journal of Physics: Conference Series*, 813:012002, April 2017. ISSN 1742-6588, 1742-6596. doi: 10.1088/1742-6596/813/1/012002.

[98] Gabriel Dan Ciocan, Olivier Teller, and Francois Czerwinski. VARIABLE SPEED PUMP-TURBINES TECHNOLOGY. page 10, 2012. ISSN 1454-2358.

[99] Weijia Yang and Jiandong Yang. Advantage of variable-speed pumped storage plants for mitigating wind power variations: Integrated modelling and performance assessment. *Applied Energy*, 237:720–732, March 2019. ISSN 03062619. doi: 10.1016/j.apenergy.2018.12.090.

[100] Weijia Yang, Per Norrlund, Linn Saarinen, Jiandong Yang, Wencheng Guo, and Wei Zeng. Wear and tear on hydro power turbines – Influence from primary frequency control. *Renewable Energy*, 87:88–95, March 2016. doi: 10.1016/j.renene.2015.10.009. URL `https://doi.org/10.1016/j.renene.2015.10.009`.

[101] Weijia Yang, Per Norrlund, Linn Saarinen, Jiandong Yang, Wei Zeng, and Urban Lundin. Wear Reduction for Hydropower Turbines Considering Frequency Quality of Power Systems: A Study on Controller Filters. *IEEE Transactions on Power Systems*, 32(2):1191–1201, March 2017. ISSN 0885-8950, 1558-0679. doi: 10.1109/TPWRS.2016.2590504. URL `https://ieeexplore.ieee.org/document/7514942/`.

[102] David Valentín, Alexandre Presas, Mònica Egusquiza, and Carme Valero. Hybridization in kaplan turbines. wear and tear assessment. *IOP Conference Series: Earth and Environmental Science*, 1079(1): 012108, September 2022. doi: 10.1088/1755-1315/1079/1/012108. URL https://doi.org/10.1088/1755-1315/1079/1/012108.

[103] Chirag Trivedi, Bhupendra Gandhi, and Cervantes J Michel. Effect of transients on francis turbine runner life: a review. *Journal of Hydraulic Research*, 51(2):121–132, 2013.

[104] Olivier Pacot, Thomas De Colombel, Claire Segoufin, Joachim Delannoy, Sebastian Leguizamon, João Delgado, Miguel Roque, and Cécile Münch-Alligné. Effect of the variable speed on the hydraulic behavior of the caniçada francis turbine, 2021.

[105] J. Yang, G. Pavesi, S. Yuan, G. Cavazzini, and G. Ardizzon. Experimental Characterization of a Pump–Turbine in Pump Mode at Hump Instability Region. *Journal of Fluids Engineering*, 137(5): 051109, May 2015. ISSN 0098-2202, 1528-901X. doi: 10.1115/1.4029572.

[106] Jun-Won Suh, Seung-Jun Kim, Jin-Hyuk Kim, Won-Gu Joo, Jungwan Park, and Young-Seok Choi. Effect of interface condition on the hydraulic characteristics of a pump-turbine at various guide vane opening conditions in pump mode. *Renewable Energy*, 154:986–1004, July 2020. ISSN 09601481. doi: 10.1016/j.renene.2020.03.017.

[107] Giovanna Cavazzini, Jean-Bernard Houdeline, Giorgio Pavesi, Olivier Teller, and Guido Ardizzon. Unstable behaviour of pump-turbines and its effects on power regulation capacity of pumped-hydro energy storage plants. *Renewable and Sustainable Energy Reviews*, 94:399–409, October 2018. ISSN 13640321. doi: 10.1016/j.rser.2018.06.018. URL https://linkinghub.elsevier.com/retrieve/pii/S1364032118304532.

[108] P-T Storli and T K Nielsen. Dynamic load on a Francis turbine runner from simulations based on measurements. *IOP Conference Series: Earth and Environmental Science*, 22(3):032056, March 2014. ISSN 1755-1307, 1755-1315. doi: 10.1088/1755-1315/22/3/032056.

[109] Chirag Trivedi, Bhupendra K. Gandhi, Michel J. Cervantes, and Ole Gunnar Dahlhaug. Experimental investigations of a model Francis turbine during shutdown at synchronous speed. *Renewable Energy*, 83:828–836, November 2015. ISSN 09601481. doi: 10.1016/j.renene.2015.05.026.

[110] Xianxun Wang, Yadong Mei, Hao Cai, and Xiangyu Cong. A new fluctuation index: Characteristics and application to hydro-wind systems. *Energies*, 9(2):114, February 2016. doi: 10.3390/en9020114. URL https://doi.org/10.3390/en9020114.

[111] Andreas Jossen. Fundamentals of battery dynamics. *Journal of Power Sources*, 154(2):530–538, March 2006. doi: 10.1016/j.jpowsour.2005.10.041. URL https://doi.org/10.1016/j.jpowsour.2005.10.041.

[112] Daniel-Ioan Stroe, Vaclav Knap, Maciej Swierczynski, Ana-Irina Stroe, and Remus Teodorescu. Operation of a grid-connected lithium-ion battery energy storage system for primary frequency regulation: A battery lifetime perspective. *IEEE Transactions on Industry Applications*, 53(1):430–438, January 2017. doi: 10.1109/tia.2016.2616319. URL https://doi.org/10.1109/tia.2016.2616319.

[113] Adam Nieslony. Rainflow Counting Algorithm, 2020. https://www.mathworks.com/matlabcentral/fileexchange/3026-rainflow-counting-algorithm.

[114] Dominique François, André Pineau, and André Zaoui. *Mechanical Behaviour of Materials, Vol II: Viscoplasticity, Damage, Fracture and Contact Mechanics*. Springer Netherlands, 1998. ISBN 978-90-481-4974-2 978-94-017-0498-4.

[115] Jorge Torres, Pablo Moreno-Torres, Gustavo Navarro, Marcos Blanco, and Marcos Lafoz. Fast Energy Storage Systems Comparison in Terms of Energy Efficiency for a Specific Application. *IEEE Access*, 6: 40656–40672, 2018. doi: 10.1109/access.2018.2854915. URL `https://doi.org/10.1109/access.2018.2854915`.

[116] Jorge Torres, Gustavo Navarro, Marcos Blanco, Mariano González-de Soto, Luis García-Tabares, and Marcos Lafoz. Efficiency Map to Evaluate the Performance of Kinetic Energy Storage Systems Used with Renewable Generation. In *2018 20th European Conference on Power Electronics and Applications (EPE'18 ECCE Europe)*, pages P–1. IEEE, 2018.